ANDRA BGR CHEVRON CRIEPI DOE ENRESA ENSI GRS IRSN JAEA NAGRA NWMO OBAYASHI SCK•CEN SWISSTOPO

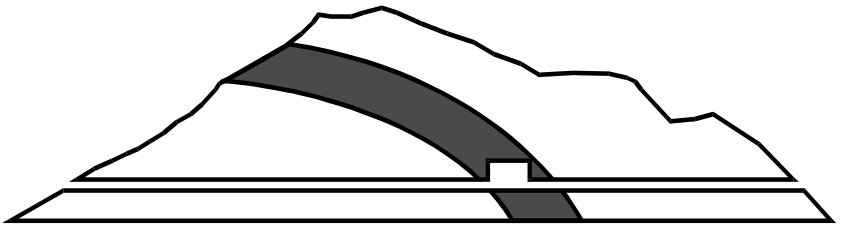

Mont Terri Project

TECHNICAL REPORT 2008-02
January 2014

SF
(Self sealing of fault and paleo-fluid flow): Synthesis report

Antoine de Haller[1], Martin Mazurek[1], Jorge Spangenberg[2], Andreas Möri[3]

[1]Rock-Water Interaction, Institute of Geological Sciences, University of Bern, Switzerland

[2]Institute of Mineralogy and Geochemistry, University of Lausanne, Switzerland

[3]swisstopo, Switzerland

Distribution:

Standard distribution:

ANDRA (S. Dewonck)

BGR (K. Schuster)

CHEVRON (P. Connolly)

CRIEPI (T. Oyama)

DOE *(P. Nair, J. Birkholzer)*

ENRESA (J.C. Mayor)

ENSI (E. Frank)

DOE (P.Nair, J. Birkholzer)

GRS (K. Wieczorek)

IRSN (J.-M. Matray)

JAEA (N. Shigita)

NAGRA (T. Vietor)

NWMO (M. Jensen)

OBAYASHI (H. Kawamura, T. Kikuchi)

SCK•CEN (F. Druyts)

SWISSTOPO (P. Bossart, A. Möri and Ch. Nussbaum)

Additional distribution:

Every organisation & contractor takes care of their own distribution.

Self-sealing of faults (SF) project: Final report

Antoine de Haller[1], Martin Mazurek[1], Jorge Spangenberg[2], Andreas Möri[3]

[1]Rock-Water Interaction, Institute of Geological Sciences, University of Bern, Switzerland
[2]Institute of Mineralogy and Geochemistry, University of Lausanne, Switzerland
[3]Swisstopo, Wabern, Switzerland

Version 27.01.2014

Abstract

Calcite, calcite-celestite and celestite veins were identifed from the bottom of the Opalinus Clay up to the Malm limestone. Most of the sampling effort for veins was focused on the NE trending Main Fault, a thrust structure related to the Jura folding and thrusting, where sub-millimeter thick calcite (±celestite) veins are common. The few accessible (no shotcrete on the gallery wall) NW trending and sub-horizontal celestite-calcite veins located below and above the Main fault were also sampled. Isotopic analyses (Sr, S, O, C) were performed on whole rock carbonate, diagenetic sulfides, evaporitic sulfates (Triassic) and vein minerals (calcite and celestite) from samples distributed along a profile from the Muschelkalk to the Malm.

Isotope data suggest that veins formed during a single geotectonic event that allowed fluids to flow across the Opalinus Clay, with the main fluid source located in the underlying Trias. Petrographic data combined with structural information indicate that vein mineral precipitation was syntectonic and most likely occurred during the Jura folding and thrusting. Sulfate-rich fluids were apparently expelled upward from the Trias aquifers (probably Keuper) through active faults and mixed with local fluids. The deep Triassic source is relatively well constrained by the strontium, sulfur, and oxygen isotopes of vein celestite, and the same data suggest the Opalinus Clay porewater was a key contributor for the precipitation of vein celestite. No data are available for the Sr and dissolved sulfate isotopic composition of the groundwater that might have been present in the Dogger-Malm at the time of vein formation and no particular isotopic imprint on the vein minerals from this aquifer has been observed. The involvement of downward flowing Tertiary seawater is not supported by the data and the geology.

Some degree of perturbation of the rock properties is observed in the Opalinus Clay in and near the Main Fault. This perturbation apparently reflects the imprint of the fluids that produced the vein mineralizations and consists of a lowering of the $\delta^{13}C$ value of the whole rock carbonate towards the values of vein calcite. In addition, weak or not straightforward lowering of the $\delta^{18}O$ value and $^{87}Sr/^{86}Sr$ ratio of the whole rock carbonate, and a depletion of the $\delta^{34}S$ of the diagenetic pyrite are observed, but doubt remains on their significance. It follows that whole rock $\delta^{13}C$ (and possibly $\delta^{18}O$) profiles across major tectonic structures might be used to highlight past fluid flow in clay-rich rocks. The use of the $^{87}Sr/^{86}Sr$ ratio of whole rock carbonate might also be effective but it is probably not reliable (or at least understood) in clay-rich rocks due to methodological problems associated with the acetic acid leach technique.

It is concluded that the Opalinus Clay apparently acted as a stable seal during most of its evolution (from 170 Ma to present), except during the Jura folding and thrusting (3-10 Ma), when tectonic strain induced transient fluid flows and mineralization in faults cutting across the Mesozoic sequence. Aside from this period of intense tectonic activity, solute transport in the Opalinus Clay has probably been dominated by diffusion, as has been demonstrated to be the case for the present. In today's situation, no hydrogeological or geochemical perturbations are recorded in the Main Fault area, and this provides arguments in favor of an efficient self-sealing capacity.

The present study also brings some new insights concerning the present day porewater composition of the Opalinus Clay. Sulfur isotope results obtained during this study on diagenetic pyrite from the Opalinus Clay show highly positive $\delta^{34}S$ values up to +58 per mil

V-CDT that indicate almost complete bacterial seawater sulfate reduction in the porewater during early diagenesis. However, other studies showed that present day porewater has a sulfate/chloride ratio similar to today's seawater and concentrations that approach seawater. It is clear from sulfur isotopes of diagenetic pyrite that the present-day sulfate content of the Opalinus Clay porewater is not inherited from the formation seawater at the time of sedimentation, and isotope data on vein celestite suggest sulfate and strontium might have diffused in the porewater from the underlying Trias evaporite, probably since sedimentation time.

Table of contents

1. Introduction

1.1 Objectives of the study

There is clear evidence that brittle structures in the Opalinus Clay at Mont Terri currently do not represent preferential flow paths. Profiles of conservative porewater tracers (Cl^-, Br^-, He, $\delta^{37}Cl$, $\delta^{18}O$, $\delta^{2}H$) do not show any perturbation near or within the Main Fault, further supporting the hydraulic irrelevance of this structure at present time (Pearson et al. 2003, Mazurek et al. 2009, 2010). Brittle structures at Mont Terri are hydraulically indistinguishable from the rock matrix, suggesting an efficient self-sealing mechanism (Meier et al. 2002). To date, overview reports on self-sealing of faults in clay-rich units applied to the nuclear waste management with some focus on the Opalinus Clay consist of Bock et al. (2010) and Fisher et al. (2013). The first reference is more focused on the engineering and geochemical perspectives, while the second explores the wide knowledge acquired in the oil and gas industry.

Calcite-celestite-pyrite veins are observed at several locations, and these represent precipitates in open fractures across which fluid flow occurred at some stage, at least transiently. Thus, the self-sealing behaviour through geological time can be evaluated by studying vein occurrences, as these commonly record past fluid flows. Vein minerals precipitate from mineralized waters that experience physico-chemical changes. These changes are commonly associated with gradients (pressure, temperature), chemical reactions with the host rock when passing from one lithology to another, and mixing of fluids from different reservoirs (with contrasting physico-chemical characteristics). Therefore, in the case of sedimentary sequences, the occurrence of vein minerals in fractures frequently indicates vertical fluid flows across lithostratigraphic units. Isotopes of certain elements that are incorporated in hydrothermal or diagenetic minerals are widely used to track past fluid flows and their source(s), and/or physico-chemical processes that occurred at the time of precipitation (e.g. Faure 1986, Ohmoto and Goldhaber 1997, Farmer and Depaolo 1997, Taylor 1997, Seal et al. 2000). Fluid flows across sedimentary sequences (including low to high permeability units) are generally transient and associated with seismic (tectonic) activity (Cox 2005). Recognition of past fluid flows, their source(s), and ideally their timing, is of interest when dealing with the paleo-hydrogeological evolution of a low-permeability formation.

Previous studies dealing with past fluid flows in the Mesozoic of Northern Switzerland are few. Studies of isotopes (C-O-S-Sr) of groundwaters and minerals/rocks of northern Switzerland include Pilot et al. (1972), Balderer et al. (1991), de Haller et al. (2011), and Wersin et al. (2013). In addition, a limited isotope study (C-O-S-Sr) has been performed on minerals and rocks in the Mont Terri underground laboratory (Waber and Schürch 2000, Pearson et al. 2003). Although a Triassic source for the aqueous sulfate involved in celestite veins found in the Opalinus Clay at Mont Terri has been suggested (Pearson et al. 2003; p. 131), no straightforward explanation has been given and the background database is small and fragmental.

The aim of this study is to improve the understanding of past fluid circulations through the Opalinus Clay at the Mont Terri laboratory by extending the petrographic and isotopic database. Two approaches were combined, one focusing on the host rock, and one on the vein fillings. Having a good understanding of the host rock isotopic composition (S-O of evaporite sulfates, S of diagenetic sulfides, C-O-Sr of carbonate fraction) can help to identify disequilibria between vein minerals and host-rock and track possible fluid sources (e.g., de

Haller et al. 2011; Mazurek et al. 2012). Vein calcite was analyzed for C-O-Sr isotopes and vein celestite for S-O-Sr isotopes.

This study is complemented by work at the Ecole et Observatoire des Sciences de la Terre in Strasbourg (France), where further mineralogical and geochemical work has been performed. Among these, K/Ar age determinations on the <0.2 µm size fraction are most noteworthy. This work is documented separately in Clauer (2011).

1.2 Regional context

The geological and structural framework of Mont Terri and Mont Russelin is summarized in Mazurek et al. (2010). Three fracture systems were identified at Mont Terri by Bossart & Thury (2008) and Nussbaum et al. (2011). Two of these systems are related to the folding and thrusting of the Jura Mountains, and the third is inherited from the Oligocene Rhine-Bresse graben system. The 1–3 meter thick Main Fault is found in the core of the Opalinus Clay and represents a thrust that was active during Jura folding and thrusting. Aside from micro-veinlets (<1mm thick) found in the Main Fault, NW trending and subhorizontal celestite-calcite veins of up to a few cm thick are documented in the Opalinus Clay (Nussbaum et al. 2011).

1.3 Sample materials

Rock materials for the SF project were obtained as follows (see also Fig. 1-1):

a. *Drilling of dedicated large-diameter boreholes penetrating faults at Mont Terri and at Mont Russelin* (BSF-004, BSF-006, BSF-11 and BSF-12). Out of these four boreholes, 3 successfully penetrated fault structures and provided cores of excellent quality, in spite of the friability of the rock materials. The drilling procedures are documented in Mazurek et al. (2010), and Tab. 4-1 of that report provides an overview of these boreholes. For geochemical purposes, samples were also taken from boreholes BSF-7, BSF-9 and BSF-11 at Mont Russelin.

b. *Continuous sampling of the tunnel wall during excavation of the Gallery 08 in Opalinus Clay at Mont Terri.* The profile length was 12.5 m and crossed the Main Fault. In total, 21 samples were taken along this profile, following the technique used for geochemical sampling in underground mines. Each sample consists of about 2 kilograms of rock chips statistically sampled on the whole length of the 0.5 or 1 meter interval, taken at about 50 cm from the floor along a corridor of about 20 cm high with the help of an electric pneumatic hammer. Not all of the samples were studied.

c. *Sampling of older core materials and of wall rock in the Mont Terri tunnels*, covering a large-scale profile from the Muschelkalk up to the Malm limestones, with a denser sampling within Opalinus Clay, in particular close to the Main Fault. These samples were taken for geochemical investigations and did not include major brittle structures. In total, 36 samples were taken.

d. *Sampling on the surface in the core of the Mont Terri anticline, locality "La Gypsière".* Five samples from the Triassic were taken.

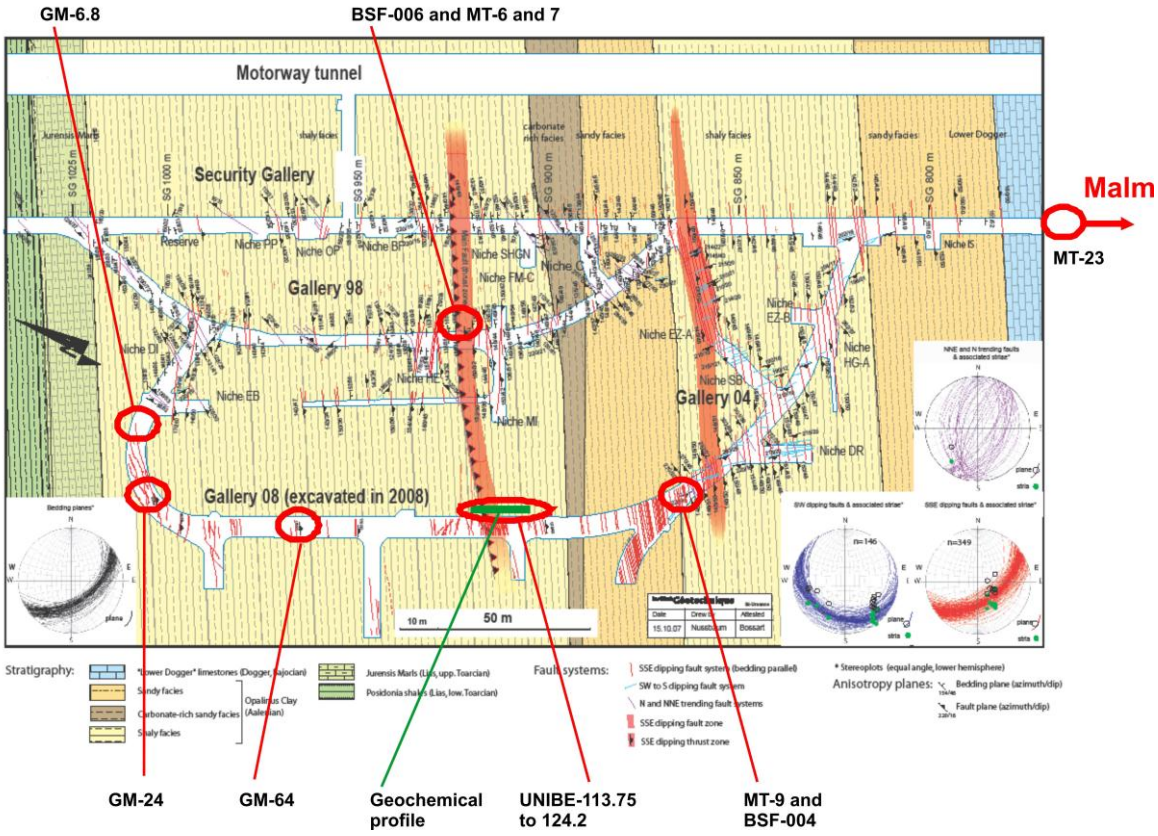

Fig. 1-1: Sampling localities of vein material at Mont Terri. The background tectonic map is from Bossart & Thury (2008)

1.4 Laboratory program

A detailed petrographic analysis (macro- and microscopic) was performed on slices from core BSF-006 (penetrating part of the Main Fault) and BSF-004 (penetrating a flat-lying celestite-calcite vein).

Petrographic and geochemical studies (in particular O and C isotopic ratios in carbonate minerals, $^{87}Sr/^{86}Sr$ in vein mineral and rock matrices, and O and S isotopes in sulfates and sulfides) were performed on vein and rock-matrix samples from the large- and small-scale profiles, the surface samples and samples from the dedicated boreholes drilled at Mont Terri and at Mont Russelin. The list of samples and the analytical program are given in Tab. 1-1. In this Table, samples are classified considering their projected position on the distance scale oriented along the emergency gallery that runs parallel to the highway tunnel and perpendicular to the Mont Terri anticline axis (Pearson et al. 2003). This distance scale increases down the stratigraphic sequence from the Malm to the Muschelkalk.

A set of samples from Mont Terri, augmented by samples of Opalinus Clay from boreholes Benken, Herdern and Kreuzlingen in northeastern Switzerland, was studied by N. Clauer at the Ecole et Observatoire des Sciences de la Terre in Strasbourg (France). A list of the samples is given in Tab. 1-2. After separation of different grain-size fractions (down to <0.2 µm), the following analytical program was conducted: mineralogical composition by X-ray

diffraction, whole-rock chemical composition (major and trace elements incl. REE), and K/Ar dating. This work is documented separately in Clauer (2011).

Tab. 1-1: Analytical program

Sample	Location	Tunnel meters [1]	Borehole Name	Borehole metering	Lithostratigraphic Unit	Type of sample	Note	Washing procedure [2]	Thin section	Isotope analyses $\delta^{34}S$	$\delta^{18}O_{SO4}$	$^{87}Sr/^{86}Sr$	$\delta^{13}C_{CO3}$	$\delta^{18}O_{CO3}$
Mont Terri:														
MT-25	Emergency gallery	35.00			Oolithe coralienne	Hand sample		---	yes			whole-rock carbonate	whole-rock carbonate	whole-rock carbonate
MT-24	Emergency gallery	255.00			Oolithe coralienne	Hand sample		---	yes			whole-rock carbonate	whole-rock carbonate	whole-rock carbonate
MT-23	Emergency gallery	275.00			Oolithe coralienne	Hand sample		---	yes			vein calcite	vein calcite	vein calcite
MT-21	Emergency gallery	675.00			Hauptrogenstein (Oolithe subcompacte)	Hand sample		---	yes			whole-rock carbonate	whole-rock carbonate	whole-rock carbonate
MT-22	Emergency gallery	725.00			Blaukalk	Hand sample		---	yes			whole-rock carbonate	whole-rock carbonate	whole-rock carbonate
BWS-E1(3.40-3.60)	Emergency gallery	779.40	BWS-E1	3.40-3.60	Lower Dogger	Piece of drill core		failed (no disaggregation)	yes			whole-rock carbonate	whole-rock carbonate	whole-rock carbonate
BWS-E4(3.25-3.45)	Emergency gallery	794.20	BWS-E4	3.25-3.45	Opalinus Clay	Piece of drill core		successful	yes	1 pyrite		whole-rock carbonate	whole-rock carbonate	whole-rock carbonate
BWS-E5(4.38-4.50)	Emergency gallery	814.50	BWS-E5	4.38-4.50	Opalinus Clay	Piece of drill core		successful	yes	1 pyrite		whole-rock carbonate	whole-rock carbonate	whole-rock carbonate
BWS-A3(28.00-28.12)	Emergency gallery	843.50	BWS-A3	28.00-28.12	Opalinus Clay	Piece of drill core		---	yes			whole-rock carbonate	whole-rock carbonate	whole-rock carbonate
BSF-004-8	Underground lab, front GAL-04	870.00	BSF-004	Slab #8	Opalinus Clay	Piece of drill core		successful	yes (slabs #9 and 12)	3 vein celestite	3 vein celestite	vein celestite		
MT-9	Underground lab: front of GAL-04	870.00			Opalinus Clay	Hand sample		successful	yes	1 pyrite		whole-rock carbonate	whole-rock carbonate	whole-rock carbonate
BWS-A2(16.85-17.17)	Emergency gallery	875.00	BWS-A2	16.85-17.17	Opalinus Clay	Piece of drill core		successful	yes	2 pyrite				
BWS-A2(2.33-2.48)	Emergency gallery	885.20	BWS-A2	2.33-2.48	Opalinus Clay	Piece of drill core		successful	yes			whole-rock carbonate	whole-rock carbonate	whole-rock carbonate
UNIBE-124.2	Underground lab: GAL-08 (124.2 m)	905.80			Opalinus Clay	Hand sample	Sampled at the front of the gallery	---	vein fraction	1 vein celestite	1 vein celestite	vein celestite-calcite	vein calcite	vein calcite
UNIBE-123.5	Underground lab: GAL-08 (123.5m)	906.50			Opalinus Clay	Geochemical sample (rock chips from gallery wall)	Out of Main Fault	successful	vein fraction			vein calcite	vein calcite	vein calcite

[1] samples are sorted according to their location projected on the security gallery metering (0 m at SE entrance). Values in ***italics*** are tentative (projection from surface outcrop).

[2] Routine method in micropaleontology: light benzine and boiling water used to disagregate the rock and recover the coarse fraction.

Tab. 1-1 (cont.)

Sample	Location	Tunnel meters [1]	Borehole Name	Borehole metering	Lithostratigraphic Unit	Type of sample	Note	Washing procedure [2]	Thin section	Isotope analyses $\delta^{34}S$	$\delta^{18}O_{SO4}$	$^{87}Sr/^{86}Sr$	$\delta^{13}C_{CO3}$	$\delta^{18}O_{CO3}$
Mont Terri:														
UNIBE-119.75	Underground lab: GAL-08 (119.75m)	910.25			Opalinus Clay	Geochemical sample (rock chips from gallery wall)	Out of Main Fault	successful	no			whole-rock carbonate	whole-rock carbonate	whole-rock carbonate
UNIBE-118.75	Underground lab: GAL-08 (118.75m)	911.25			Opalinus Clay	Geochemical sample (rock chips from gallery wall)	Out of Main Fault	successful	no			whole-rock carbonate	whole-rock carbonate	whole-rock carbonate
UNIBE-118.25	Underground lab: GAL-08 (118.25m)	911.75			Opalinus Clay	Geochemical sample (rock chips from gallery wall)	Out of Main Fault	successful	vein fraction			vein calcite / bivalve shell / echinoderm	vein calcite / bivalve shell /	vein calcite / bivalve shell /
UNIBE-117.25	Underground lab: GAL-08 (117.25m)	912.75			Opalinus Clay	Geochemical sample (rock chips from gallery wall)	Main fault	successful	vein fraction					
UNIBE-116.25	Underground lab: GAL-08 (116.25m)	913.75			Opalinus Clay	Geochemical sample (rock chips from gallery wall)	Main fault	successful	vein fraction			vein calcite (±celestite)	vein calcite	vein calcite
MT-8	Underground lab: HE-D	915.00	BPC-1	between 0 and 5	Opalinus Clay	Piece of drill core		successful	no	2 pyrite				
UNIBE-114.75	Underground lab: GAL-08 (114.75m)	915.25			Opalinus Clay	Geochemical sample (rock chips from gallery wall)	Main fault	successful	vein fraction			whole-rock carbonate	whole-rock carbonate	whole-rock carbonate
UNIBE-113.75	Underground lab: GAL-08 (113.75m)	916.25			Opalinus Clay	Geochemical sample (rock chips from gallery wall)	Main fault	successful	vein fraction			vein calcite	vein calcite	vein calcite
BSF-006-(13)	Underground lab: Main fault, window ENE	923.00	BSF-006	Slab #13	Opalinus Clay	Piece of drill core	Main fault	successful	yes (in slab #11)	2 pyrite		vein calcite	vein calcite	vein calcite
BSF-006-(7-8)	Underground lab: Main fault, window ENE	923.00	BSF-006	Slab #7-8	Opalinus Clay	Piece of drill core	Main fault	successful	yes (in slab #11)	2 pyrite				
MT-6	Underground lab: Main fault, window ENE	923.00			Opalinus Clay	Hand sample	Main fault	successful	yes	5 pyrite		vein calcite	vein calcite	vein calcite
MT-7	Underground lab: Main fault, window ENE	925.00			Opalinus Clay	Hand sample	Main fault	successful	yes	1 pyrite		whole-rock carbonate	whole-rock carbonate	whole-rock carbonate
BWS-A1(1.20-1.40)	Emergency gallery	949.30	BWS-A1	1.20-1.40	Opalinus Clay	Piece of drill core		successful	yes	3 pyrite				
GM-64	Underground lab: GAL-08 (64m)	967.00			Opalinus Clay	Hand sample		---	yes	1 vein celestite	1 vein celestite	vein celestite-calcite		

[1] samples are sorted according to their location projected on the security gallery metering (0 m at SE entrance). Values in ***italics*** are tentative (projection from surface outcrop).

[2] Routine method in micropaleontology: light benzine and boiling water used to disagregate the rock and recover the coarse fraction.

Tab. 1-1 (cont.)

Sample	Location	Tunnel meters [1]	Borehole Name	Borehole metering	Lithostratigraphic Unit	Type of sample	Note	Washing procedure [2]	Thin section	Isotope analyses $\delta^{34}S$	$\delta^{18}O_{SO4}$	$^{87}Sr/^{86}Sr$	$\delta^{13}C_{CO3}$	$\delta^{18}O_{CO3}$
Mont Terri:														
GM-24	Underground lab: GAL-08 (24 m)	1003.00			Opalinus Clay	Hand sample		---	yes	1 vein celestite	1 vein celestite	vein celestite-calcite		
BWS-A6(19.55-19.75)	Emergency gallery	1003.50	BWS-A6	19.55-19.75	Opalinus Clay	Piece of drill core		successful	yes	9 pyrite		whole-rock carbonate	whole-rock carbonate	whole-rock carbonate
GM-6.8	Underground lab: GAL-08 (6.8 m)	1010.00			Opalinus Clay	Hand sample		---	yes	1 vein celestite	1 vein celestite	vein celestite-calcite	vein celestite-calcite	vein celestite-calcite
BWS-E6(5.00-5.15)	Emergency gallery	1022.10	BWS-E6	5.00-5.15	Jurensis Marl	Piece of drill core		successful	yes	4 pyrite		whole-rock carbonate	whole-rock carbonate	whole-rock carbonate
BWS-E7(4.95-5.10)	Emergency gallery	1050.60	BWS-E7	4.95-5.10	Posidonia Shale	Piece of drill core		failed (no disaggregation)	yes			whole-rock carbonate	whole-rock carbonate	whole-rock carbonate
BWS-E8(4.70-5.10)	Emergency gallery	1080.40	BWS-E8	4.70-5.10	Obtusus Clay & Obliqua layer	Piece of drill core		successful	yes	2 pyrite		whole-rock carbonate	whole-rock carbonate	whole-rock carbonate
BWS-E9(4.80-5.10)	Emergency gallery	1121.90	BWS-E9	4.80-5.10	Rhaetian / Gryphaea limestone	Piece of drill core		successful	yes (of the limestone)	4 pyrite		whole-rock carbonate (plus limestone and shale fractions)	whole-rock carbonate	whole-rock carbonate
MT-3	Mont Terri, La Gypsière	*1150.00*			Rhaetian	Hand sample		---	yes	3 evaporite gypsum	3 evaporite gypsum	evaporite gypsum		
MT-4	Mont Terri, La Gypsière	*1150.00*			Rhaetian	Hand sample		---	yes					
MT-1	Mont Terri, near La Gypsière	*1350.00*			Rhaetian	Hand sample		---	yes					
MT-2	Mont Terri, near La Gypsière	*1350.00*			Rhaetian	Hand sample		---	yes					
MT-20	Emergency gallery	1550.00			Trigonodus-Dolomite	Hand sample		---	yes	1 evaporite gypsum / anhydrite	1 evaporite gypsum / anhydrite	whole-rock carbonate	whole-rock carbonate	whole-rock carbonate
Mont Russelin:														
MR-SF7	Tunnel		SF7	1.55	Opalinus Clay	Piece of drill core		successful	yes			vein calcite-celestite	vein calcite	vein calcite
SF9 (1.8)	Tunnel		SF9	1.8	Opalinus Clay	Piece of drill core		---	yes					
BSF11 (13-15)	Tunnel		BSF11	1.05	Opalinus Clay	Piece of drill core		---	yes	1 vein celestite	1 vein celestite	vein celestite-calcite	vein calcite	vein calcite

[1] samples are sorted according to their location projected on the security gallery metering (0 m at SE entrance). Values in ***italics*** are tentative (projection from surface outcrop).

[2] Routine method in micropaleontology: light benzine and boiling water used to disagregate the rock and recover the coarse fraction.

Tab. 1-2: Samples selected for mineralogical and geochemical studies at the Ecole et Observatoire des Sciences de la Terre in Strasbourg (France)

Location	Depth / sample ID	Mass, g	Remarks
Mont Terri	MF-1	200	Fault rock from Main Fault; contains substantial fraction of harder components (wallrocks)
Mont Terri	MF-2	450	Fault rock from Main Fault, soft, dark, clay-rich, only minor contamination by wallrock; rich in fault gouge
Mont Terri	BSF-006-C1	138	Core SF-6, slabs 15, 16, 18, 23-28. Fault gouge, carefully separated from wallrocks. Only 2-4 mm thick horizon of very soft and cohesionless rock
Mont Terri	BSF-006-C2	935	Core SF-6, slabs 15, 16, 19-22. Shear zone, ca. 5 cm thick, bounded by fault-gouge horizons, embedded in undeformed matrix. Strongly reduced cohesion, but harder than fault gouge
Mont Terri	BSF-006-C3	1130	Core SF-6, slabs 15, 16, 19-22. Unfractured material, 0 - 5 cm away from shear zone
Mont Terri	DR-1	1200	DR drillcore from 2.78-3.08 m, about 7 m away from the next major tectonic fault zone. Benchmark matrix sample; contains some slickensides
Benken	645.05	340	very clay-rich lower part of OPA
Benken	571.4	1500	carbonate-rich layer
Herdern	1727.12	340	shale with numerous silt lenses
Kreuzlingen	2173.35	1380	Heterogeneous, hardground sample, partly brownish

2. Methodology

2.1 Drilling of dedicated boreholes

The preservation of friable materials such as clay-rich sedimentary rocks affected by brittle deformation is challenging when samples are obtained by core drilling. The strategy and the methodology of drilling-site selection and drilling procedures applied to obtain some of the core materials studied in this report are described in Mazurek (2010) and are not repeated here.

2.2 Separation of materials for isotopic analysis

Coarse and dense materials (sulfides, fossils, vein fragments, cemented sandy layers) in clay-rich rocks were separated with a technique that is routinely used for micro-paleontological studies of clay-rich rocks. 200 to 700 grams of coarsely crushed (<3 cm size) rock sample were dried at 80 °C for more than 12 hours and then covered with gasoline for 0.5 to 1 hour in a 1 L beaker. After removal of the supernatant gasoline, the sample was immediately covered with boiling water and stirred with a glass rod. The boiling water induces strong boiling of the gasoline absorbed into the samples, which provokes disaggregation. Then, the fine fraction (mostly clay) was removed by washing with water in the beaker so that the coarse and heavy particles stayed at bottom. The coarse and heavy fraction was finally collected in a paper cone, rinsed with fuel alcohol and put to dry into an oven at 80 °C. If the sample did not completely disaggregate, the full procedure was repeated. In certain cases, the remaining clay was removed by putting the sample into an ultrasonic bath for 15-25 minutes before washing with water. The different pyrite fractions, fossils, or vein fragments were separated from the coarse and heavy concentrate by hand picking under binocular lenses following morphological criteria.

Except for vein celestite recovered in washed residues obtained by the method described above, sulfate minerals (evaporite gypsum and vein celestite) were separated with a small dentist-like diamond drill from cut rock chips (>3 mg for each aliquot).

2.3 Analytical methods

Sulfate from powdered celestite was purified through complete dissolution in a 1M HCl solution followed by precipitation as $BaSO_4$ with the addition of a few milligrams of $BaCl_2$. The supernatant solution was then pipetted and the precipitate washed with distilled water and dried. Gypsum powder samples were heated at 110 °C for one day to convert them to anhydrite.

Sulfur isotopes of sulfide and sulfate minerals and oxygen isotopes of sulfate minerals were measured at the University of Lausanne (Switzerland). The sulfur isotope analyses were performed using an on-line elemental analyzer Carlo Erba 1108 coupled, through a continuous helium flow interface, to a Thermo Finnigan (Bremen, Germany) DELTA S isotope ratio mass spectrometer (EA/IRMS) system, according to the technique described by Giesemann et al. (1994). The 0.1 to 0.2 mg sulfur mineral powders were wrapped in tin capsules and completely converted to SO_2 under a flow of helium and oxygen by flash combustion at 1030°C, in an oxidation-reduction quartz tube packed with oxidizing (WO_3)

and reducing (elemental Cu) agents. A helium stream carried the gases produced during the combustion through a water trap (10 cm glass tube packed with anhydrous $MgClO_4$) and a chromatographic teflon column (6x4 mm, 80 cm) at 70°C, for separation of SO_2, which then enter the isotope ratio mass spectrometer. Reference SO_2 gas was inserted as pulses of pure standard gas, which is calibrated against the NBS-123 zinc sulfide ($\delta^{34}S$ value of +17.1‰) international standard. The stable isotope composition of sulfur is reported in delta (δ) notation as the per mil (‰) deviations of the isotope ratio relative to the Vienna Canyon Diablo Troilite (V-CDT) standard:

$$\delta = [(R_{sample} - R_{standard})/R_{standard}] \times 1000$$

where R is the ratio of the heavy to light isotopes ($^{34}S/^{32}S$). The reproducibility of the EA-IRMS, assessed by replicate analyses of laboratory standard materials (synthetic barium sulfate, +12.5‰ $\delta^{34}S$; natural pyrite, –7.0‰ $\delta^{34}S$), was better than ±0.2‰ (1σ error). The accuracy of the $\delta^{34}S$ analyses is checked periodically by analyses of the international reference materials IAEA S1 and S2 silver sulfide (-0.3‰ and +21.7‰ $\delta^{34}S$), and NBS-123.

The oxygen isotopic composition of the sulfates was measured with a Thermo Finnigan high temperature conversion elemental analyzer (TC/EA) coupled to a Delta Plus XL isotope ratio mass spectrometer. The 0.1 to 0.2 mg sulfate powders were wrapped in silver capsules and completely reduced in the TC/EA, in which oxygen is converted to CO under a flow of helium at 1470°C in a glassy carbon reactor with an outer ceramic mantel tube of aluminum oxide. A helium stream carried the gases produced during the combustion through a chromatographic column (6x4 mm, 80 cm) at 80°C, for separation of CO, which then enter the isotope ratio mass spectrometer. Reference CO gas was inserted as pulses of pure standard gas. The oxygen isotope ratios ($\delta^{18}O$) are reported relative to the Vienna Standard Mean Ocean Water (V-SMOW). The reproducibility of the TC/EA/IRMS measurements, assessed by replicate analyses of the laboratory barium sulfate standards (UNIL, 14.0‰; UVA, 12.4‰) was better than ±0.3‰ (1σ error). The accuracy of the TC/EA/IRMS $\delta^{18}O$ analyses is checked periodically by analyses of international reference barium sulfates NBS-127 (+9.9‰), IAEA SO-5* (+3.5‰) and S0-6 (-10.8‰).

The stable C and O isotope composition of whole rock and vein carbonate was measured at the University of Bern (Switzerland) on a Finnigan Delta V Advantage mass spectrometer equipped with an automated carbonate preparation system (Gas Bench-II). Results are reported relative to the V-PDB standard; standardization was accomplished using international standards NBS 19 and NBS 18. The long-term precision of $\delta^{13}C$ and $\delta^{18}O$ is 0.052‰ and 0.063‰ (1σ error; n = 1156) respectively.

Sr isotope measurements were performed at the University of Bern (Switzerland). Celestite crystals (ca. 0.5-1 mg) were dissolved in distilled HNO_3, while clay-carbonate mixtures (typically milled whole rock sample) were leached in dilute (ca. 0.5 M) acetic acid for 60 to 90 minutes at 25 °C, the Ca acetate being then evaporated to dryness and re-dissolved in HNO_3. The Sr was separated from the matrix nitrates using Sr-Spec resin in miniaturized columns. The resulting pure Sr fraction was diluted as necessary and Sr isotope ratios analyzed on a Nu Instruments multicollector ICP mass spectrometer. The external reproducibility of the NIST SRM 987 during the period of the present analyses was 0.710235 ± 0.000020 (2σ error).

2.4 BET and density measurements

Density (dry) and external-surface (BET) measurements were performed on subsamples of the cores BSF-006 and BSF-004. Subsamples were selected in three classes of tectonic imprint grading from intact "matrix" to "fault gouge". BSF-006 was drilled in the clay-rich facies of the Opalinus Clay, within the Main Fault, while BSF-004 was drilled in the sandy facies, crosscutting a celestite-calcite vein. No shear imprint is present in BSF-004 and therefore only intact "matrix" was sampled for this borehole.

Powdered rock material (grain size ≤ 2 mm) for the measurement of specific surface area was weighed to an accuracy of 0.001 grams and thoroughly desorbed of primary adsorbed gases by heating under vacuum at 150 ºC for approximately 1 hour. Nitrogen adsorption isotherms of the powdered samples were measured in equilibrium with liquid nitrogen using a Coulter SA 3100 surface analyser. The N-surface area was calculated using the Brunauer, Emmet and Teller method (BET; Brunauer *et al.* 1938) for a pressure range of P/P_0 from 0 to 1. The specific surface area (expressed as m^2/g) was obtained from the N-surface area and the sample weight.

Density measurements were performed on rock chips weighing between 3 and 31 g using the paraffin displacement method (see Waber 2008). Density of fault gouge could not be measured because the material has no cohesion.

3. Structural-petrographic characterization of sample materials

3.1 Samples from the large- and small-scale geochemical profiles

A petrographic documentation of the samples from the large- and small-scale profiles is provided in Tab. 3-1. It is based on thin and polished sections and/or on the coarse washed fraction of clay-rich rocks. Veins hosted by the Opalinus Clay are filled with calcite, celestite, and pyrite, while only calcite has been observed in the Malm limestone.

The coarse residue of Opalinus Clay samples consists essentially of bioclasts (bivalve shells, echinoderms, gasteropods, foraminifera, ostracods, ammonites, and crabs), fragments of cemented sandy laminae, small (<1mm) fragments of carbonaceous matter, diagenetic pyrite and sphalerite, and vein fragments. Fig. 3.1 (A to C) shows typical examples of unsorted coarse fractions obtained through washing of Opalinus Clay samples. Fig. 3.1(D) shows the morphologies of diagenetic pyrite found in Opalinus Clay: flat fine-grained, framboidal aggregate, columnar, pyritized ammonite and gasteropods, and medium- and fine-grained masses.

Fig. 3-2 shows thin sections of vein fragments collected by the washing procedure of Opalinus Clay rock samples. The presence of these small veins was not visible on the outcrop but should be detectable in thin section. Vein calcite and celestite are frequently fibrous due to syn-tectonic growth, vein thickness being generally <1mm. Calcite is much more common than celestite in these small veins. Such small vein fragments were found in most of the geochemical samples taken from the new Gallery 08 (series of samples labeled UNIBE-113.5 to 123.5), within and outside the main boundaries of the Main Fault. This fits with field observation indicating that the Main Fault is much more diffuse in this area of the underground laboratory than in the niches of Gallery 98, where the Main Fault has sharp boundaries. The presence of thin calcite-dominated veins as sampled in the Main Fault area is not documented outside the Main Fault.

Veins that are recognized in Opalinus Clay outcrops outside the Main Fault are generally thicker, a few millimeters to about 2 cm (sample GM6.8), and contain celestite, sometimes without calcite. They tend to be oriented NW or subhorizontal (Waber and Schürch 2000; Nussbaum et al. 2011). Examples of thick celestite-calcite veins are shown in Figs. 3-3 and 3-4. Fig. 3-3 shows that the texture of celestite-calcite veins can be complex. Calcite and celestite apparently precipitated nearly at the same time. The rhomb-shaped open space in Fig. 3-3B corresponds to a micro pull-apart feature and indicates that the latest shear tectonic activity occurred after the main stage of vein formation. Very small crystals of calcite (Fig. 3-3C) and celestite (Fig. 3-3D) freely growing in or filling (Fig. 3-3B) related extension cracks indicate these open structures are original features and not artifacts created during the construction of the gallery or the thin section preparation. Fig. 3-4 shows the range of typical celestite morphologies, from fibrous syn-tectonic growth (A and B), to free prismatic growth (C and D). A view of the calcite veins that cut the Malm (Oolithe Coralienne) is shown in Fig. 3-4E,F. The presence of a stylolite joint in the vein calcite suggests that the calcite vein has formed before or at the beginning of a major compressional event.

Fig. 3-5 shows massive evaporite gypsum and anhydrite from Trias. Sample MT-20 is from Muschelkalk and was sampled in the emergency gallery. It shows an intergrowth of anhydrite

in gypsum as patches in the fine-grained host dolomite. Sample MT-3 is from the surface outcrop called "La Gypsière", on top of the Mont Terri chain, and consists of massive gypsum of Keuper age.

Diagenetic pyrite is widespread in the sedimentary sequence (except in the sulfate-rich Trias), and marcasite is abundant at the Keuper-Lias boundary (Rhaetian-Gryphaea Limestone contact). Trace amounts of diagenetic sphalerite occur in some of the Opalinus Clay samples. The detailed petrography of the opaque minerals present in the Opalinus Clay is presented in sections 3.2 and 3.3, which are based on the overcored boreholes BSF-006 and BSF-004.

Tab. 3-1: Petrographic characteristics of the samples from the large- and small-scale profiles

Sample	Tunnel meters [1]	Lithostratigraphic Unit	Description [2]
Mont Terri:			
MT-25	35.00	Oolithe coralienne	Oolithic limestone.
MT-24	255.00	Oolithe coralienne	Oolithic limestone cut by minor calcite veins. No opaque minerals nor organic matter. Stilolites are later than calcite cement, and possibly after veins.
MT-23	275.00	Oolithe coralienne	Oolithic limestone cut by calcite veins. Sample is close to a NE trending fault (50 m strike-slip displacement). Stilolites overprint veins.
MT-21	675.00	Hauptrogenstein (Oolithe subcompacte)	Oolithic limestone. Calcite cement. Few calcite veins. Very rare pyrite.
MT-22	725.00	Blaukalk	Sandy bioclastic limestone (clast supported with calcite cement). Some brownish organic matter and opaque mineral (not det.).
BWS-E1(3.40-3.60)	779.40	Lower Dogger	Shaly sandstone. Relatively homogeneous shaly sandstone. Calcite cemented where less clay-rich. Very few fossils. Disseminated opaque minerals.
BWS-E4(3.25-3.45)	794.20	Opalinus Clay	Sandy shale. Calcite- and quartz-cemented sandy beds contain detrital qtz, mus, K-feld, carbonaceous matter. Locally, py beds.
BWS-E5(4.38-4.50)	814.50	Opalinus Clay	Sandy shale. Thin sandy beds cemented by calcite contain detrital quartz, muscovite, and minor K-feldspar. Minor bioclasts. Some framboidal pyrite.
BWS-A3(28.00-28.12)	843.50	Opalinus Clay	Bioclastic shale (alternance of shaly and bioclastic-sandy beds). Contains bivalves, echinoderms, py.
BSF-004-8	870.00	Opalinus Clay	Shale (sandy facies). Sandy beds (<1 mm thick) are cemented by calcite, pyrite and sphalerite. The sandy fraction consists essentially of quartz and muscovite. A <1 cm thick celestite-calcite vein crossscuts the sample.
MT-9	870.00	Opalinus Clay	Sandy shale. Sampled close to celestite vein (c.f. BSF-004). Contains some bivalve, detrital qtz, mus, K-feld and carbonaceous matter. Disseminated framboidal pyrite.
BWS-A2(16.85-17.17)	875.00	Opalinus Clay	Shale (sandy facies). Contains calcite-cemented sand beds (<1mm thick), framboidal pyrite, rare bioclasts (bivalves, crabs, foraminifera, gasteropods). Up to 3 mm thick calcite (celestite?) veins.
BWS-A2(2.33-2.48)	885.20	Opalinus Clay	Shaly sandstone. Contains almost no fossils. Calcite-cemented sandy fraction contains qtz, mus, feld, biot, carbonaceous matter. Minor fine framboidal py.
UNIBE-124.2	905.80	Opalinus Clay	Calcite-celestite vein in bioclastic shale. Dips towards N125°E at 55°. Syntectonic massive granular to radiated acicular celestite with calcite. Pyrite (?) only in host rock.
UNIBE-123.5	906.50	Opalinus Clay	Shaly facies with few sandy beds. Contains bivalves, pieces of cemented sandstone, ostracods, ammonites, gasteropods, echinoderms, crabs, pyrite. Few calcite veins.

[1] samples are sorted according to their location projected on the security gallery metering (0 m at SE entrance). Values in ***italics*** are tentative (projection from surface outcrop).

[2] Abbreviations: bt = biotite, feld = feldspar, mc = marcasite, mus = muscovite, py = pyrite, qtz = quartz, ttn = titanite.

Tab. 3-1 (cont.)

Sample	Tunnel meters [1]	Lithostratigraphic Unit	Description [2]
Mont Terri:			
UNIBE-119.75	910.25	Opalinus Clay	Shaly facies with few sandy beds. Contains pieces of cemented sandstone, bivalves, ostracods, gasteropods, echinoderms, pyrite, minor sphalerite. No veins.
UNIBE-118.75	911.25	Opalinus Clay	Shaly facies with few sandy beds. Contains bivalves, ostracods, pieces of cemented sandstone, foraminifers, coal, ammonite, echinoderms (spines), pyrite. No veins.
UNIBE-118.25	911.75	Opalinus Clay	Shaly facies. Contains bivalves, echinoderms, ostracods, ammonites, foraminifers, pyrite, minor sphalerite, small rounded clasts of pinkish micrite(?). Calcite veins (fibrous).
UNIBE-117.25	912.75	Opalinus Clay	Shaly facies with rare sandy beds. Contains bivalves, ostracods, crabs, foraminifera, ammonite, pyrite, and minor sphalerite. Calcite veins (fibrous).
UNIBE-116.25	913.75	Opalinus Clay	Shaly facies (very rare sandy beds). Contains bivalves, ostracods, coal, echinoderms (spines), pyrite, minor sphalerite. Rare small rounded clasts of pinkish micrite(?) with pyrite. Calcite (±celestite)-pyrite veins (fibrous).
MT-8	915.00	Opalinus Clay	Bioclastic shale. No thin section.
UNIBE-114.75	915.25	Opalinus Clay	Shaly facies (rare sandy layers?). Contains bivalves, gasteropods, ostracods, foraminifers, ammonite, pyrite, minor sphalerite, limestone (micritic) clasts. Calcite veins (fibrous).
UNIBE-113.75	916.25	Opalinus Clay	Shaly facies with few sandy beds. Contains pieces of cemented sandstone, bivalves, ammonite, foraminifers, ostracods, crabs, gasteropods, pyrite. Calcite veins (fibrous).
BSF-006-(13)	923.00	Opalinus Clay	Shale (shaly facies). Contains bivalves, gasteropods, foraminifera, and ostracods. Little pyrite. Calcite veins (<1mm thick).
BSF-006-(7-8)	923.00	Opalinus Clay	Shale (shaly facies). Contains bivalves, gasteropods, foraminifera, and ostracods. Pyrite.
MT-6	923.00	Opalinus Clay	Shale (shaly facies). Fault gouge and rock clasts near hanging wall of Main fault zone. Contains bivalves, crabs, foraminifera, ammonites, fish bones, gasteropods, and calcite (py) veins.
MT-7	925.00	Opalinus Clay	Bioclastic shale within Main fault. Contains bivalve, crabs, gasteropods, and minor py.
BWS-A1(1.20-1.40)	949.30	Opalinus Clay	Shale (shaly facies). Contains bivalves, gasteropods, foraminifera, and ostracods. Thin sandy beds cemented by calcite and pyrite.
GM-64	967.00	Opalinus Clay	Calcite-celestite vein in shale. At least 2 generations of syntectonic celestite and calcite. Late strike-slip (pull-apart) open-spaces partially filled by cel-cal. Framboidal pyrite in host rock. No opaque mineral in veins.

[1] samples are sorted according to their location projected on the security gallery metering (0 m at SE entrance). Values in ***italics*** are tentative (projection from surface outcrop).

[2] Abbreviations: bt = biotite, feld = feldspar, mc = marcasite, mus = muscovite, py = pyrite, qtz = quartz, ttn = titanite.

Tab. 3-1 (cont.)

Sample	Tunnel meters [1]	Lithostratigraphic Unit	Description [2]
Mont Terri:			
GM-24	1003.00	Opalinus Clay	1.3 cm thick celestite vein, flanked by sliken side on both sides (celestite crystals are sharply cut). Celestite crystals are idiomorphic, slightly zoned in polarized light and embedded in clay and carbonate (in part bioclastic). Part of the celestite is fractured and cemented by celestite and calcite in sigmoidal open-spaces. Minor amount of py.
BWS-A6(19.55-19.75)	1003.50	Opalinus Clay	Shale (shaly facies). Contains bivalves, gasteropods, foraminifera, ostracods, and crabs. Small py lenses. Storage dehydration cracks partially filled with gypsum (from py oxidation).
GM-6.8	1010.00	Opalinus Clay	2cm thick celestite vein, flanked by sliken side on both sides (celestite crystals are sharply cut). Celestite crystals are idiomorphic, slightly zoned in polarized light, and embedded in clay and carbonate (in part bioclastic). Minor amount of py.
BWS-E6(5.00-5.15)	1022.10	Jurensis Marl	Shale (shaly facies). Contains few bioclasts. Diagenetic py close to dehydration cracks is oxidized (-> Fe-hydrox and gypsum).
BWS-E7(4.95-5.10)	1050.60	Posidonia Shale	Bituminous shale. Well bedded homogeneous mixture of fine grained carbonate, clay (low birefringence), brown organic matter, and opaque (pyrite, carbonaceous matter?). Some calcite veins.
BWS-E8(4.70-5.10)	1080.40	Obtusus Clay & Obliqua layer	Bioclastic shale. Contains bivalves, echinoderms, glauconite. Pyrite is oxidized (Fe-hydrox + gypsum) close to dehydration cracks.
BWS-E9(4.80-5.10)	1121.90	Rhaetian / Gryphaea limestone	Black shale and bioclastic limestone. Black shale very rich in py-mc, while limestone moderately. Limestone contains echinoderms, bivalves, foraminifers, and brownish organic matter.
MT-3	*1150.00*	Rhaetian	Evaporite. Fibrous massive gypsum. Banded zones with relicts of anhydrite (as inclusions), brownish clay(?), and carbonate.
MT-4	*1150.00*	Rhaetian	Massive gypsum with anhydrite relicts (as inclusions) and clay rock.
MT-1	*1350.00*	Rhaetian	Bedded dolomite showing little holes (probably after anhydrite dissolution; few remnants of gypsum).
MT-2	*1350.00*	Rhaetian	Same as sample MT-1
MT-20	1550.00	Trigonodus-Dolomite	Bedded medium to fine-grained dolomite with inclusions of anhydrite-gypsum (<2cm), locally cut by gypsum veins.

[1] samples are sorted according to their location projected on the security gallery metering (0 m at SE entrance). Values in ***italics*** are tentative (projection from surface outcrop).

[2] Abbreviations: bt = biotite, feld = feldspar, mc = marcasite, mus = muscovite, py = pyrite, qtz = quartz, ttn = titanite.

Tab. 3-1 (cont.)

Sample	Tunnel meters [1]	Lithostratigraphic Unit	Description [2]
Mont Russelin:			
MR-SF7		Opalinus Clay	Bioclastic shale (shaly facies) cut by syn-tectonic calcite-celestite veins in fault zone. Opaque minerals (py?) in the host rock
SF9 (1.8)		Opalinus Clay	Sandy shale cut by a calcite vein. Calcite vein cuts bedding. Sandy (quartz, muscovite, Kfeld) beds (mm) are cemented by calcite and pyrite(?). Few bioclasts.
BSF11 (13-15)		Opalinus Clay	Bioclastic shale (shaly facies) cut by syn-tectonic calcite-celestite veins in fault zone. Pyrite in the host rock.

[1] samples are sorted according to their location projected on the security gallery metering (0 m at SE entrance). Values in ***italics*** are tentative (projection from surface outcrop).

[2] Abbreviations: bt = biotite, feld = feldspar, mc = marcasite, mus = muscovite, py = pyrite, qtz = quartz, ttn = titanite.

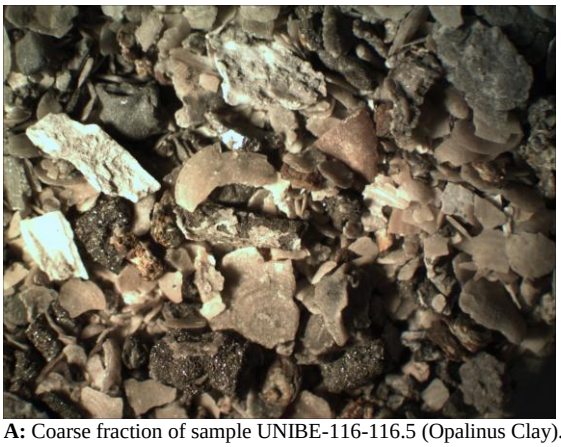

A: Coarse fraction of sample UNIBE-116-116.5 (Opalinus Clay). It includes pieces of shell, echinoderms, diagenetic pyrite, and calcite vein fragments. Length of picture is 15 mm.

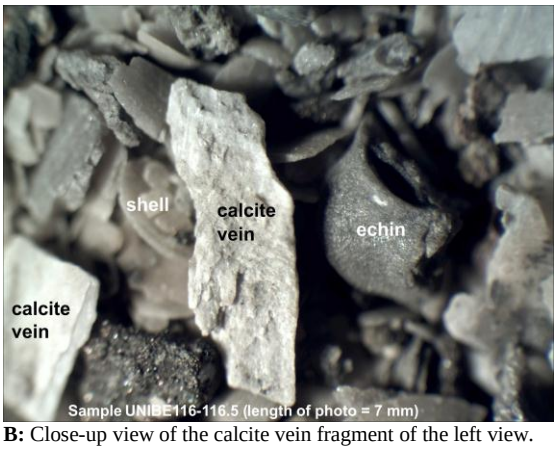

B: Close-up view of the calcite vein fragment of the left view. Length of picture is 7 mm.

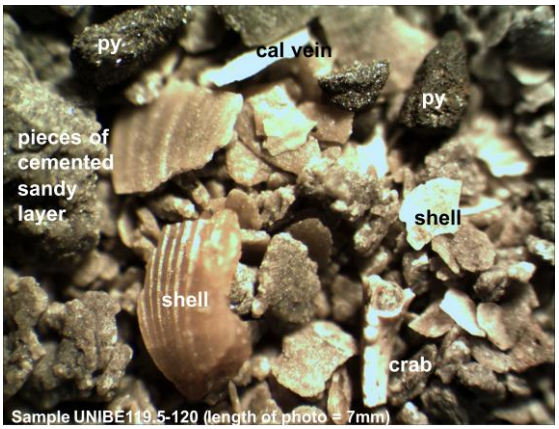

C: Coarse fraction of sample UNIBE-119.5-120 (Opalinus Clay). It includes pieces of shell and cemented sandy layers, fine-grained pyrite clusters (py), a piece of crab, and calcite vein fragments (cal vein). Length of picture is 7 mm.

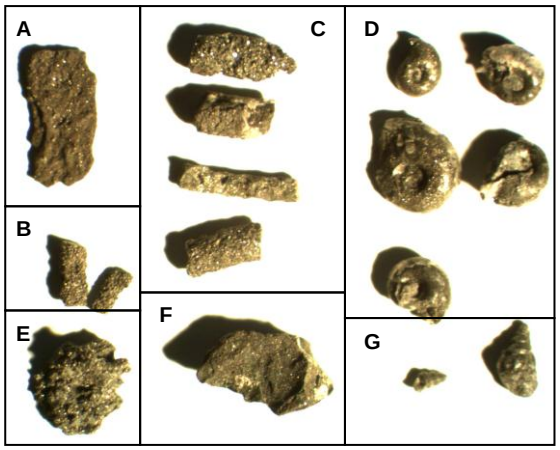

D: Diagenetic pyrite from sample UNIBE 113.5-114 (Opalinus Clay). Length of picture frame is 15 mm. Each lettered field correspond to a type of diagenetic pyrite: A) flat, fine-grained; B) framboidal aggregate; C) columnar; D) pyritized ammonite; E) massive medium-grained; F) massive, fine-grained; G) pyritized gasteropods.

Fig. 3-1: Petrography of typical coarse fractions from Opalinus Clay

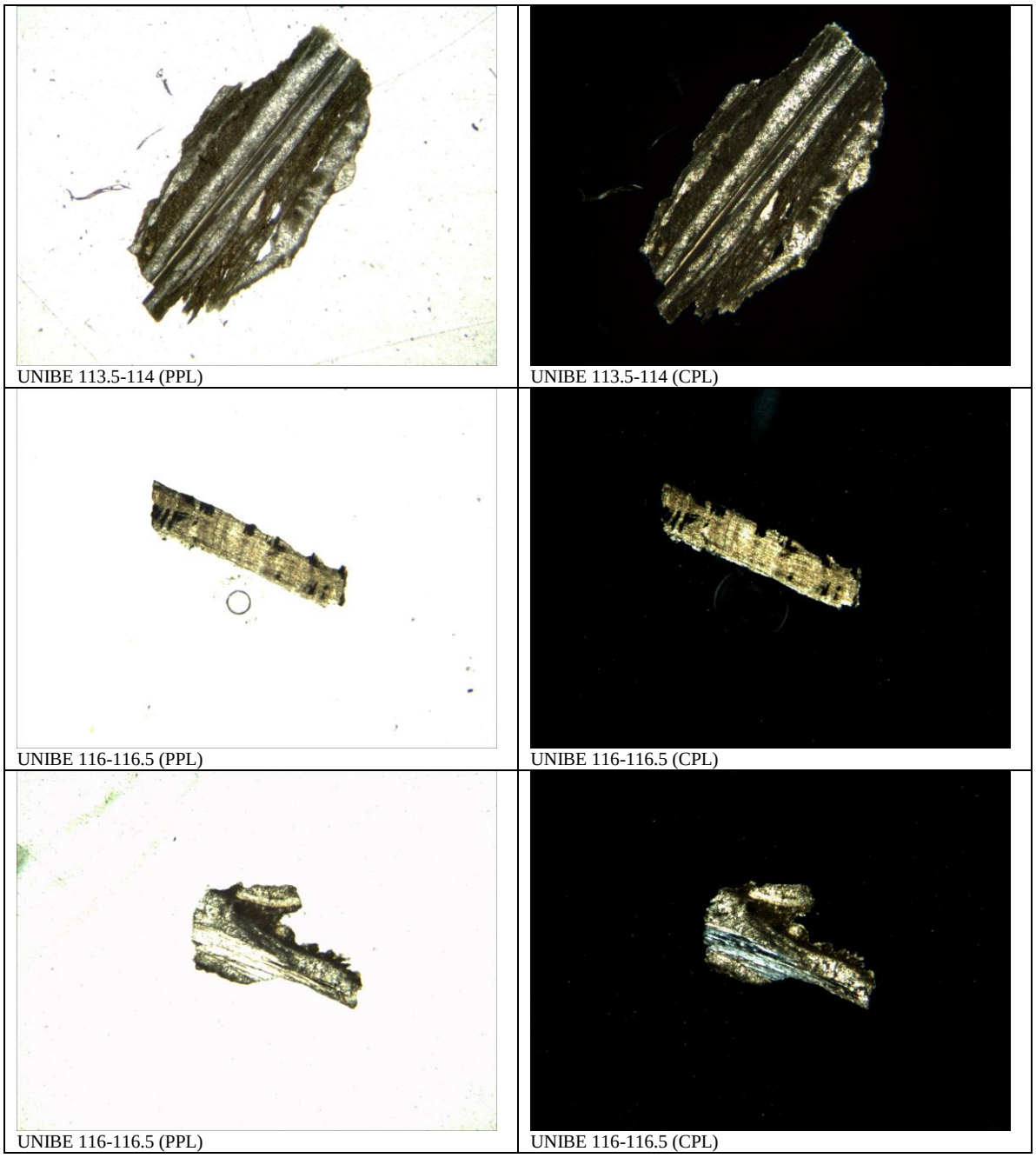

Fig. 3-2: Thin section views of typical vein samples from Opalinus Clay recovered by the washing procedure. In all the cases, the length of the picture is 3.5 mm. PPL = plane polarized light, CPL= crossed polarized light. All the samples are calcite veins, with celestite in the lower sample UNIBE 116-116.5 (grey birefringence color in CPL)

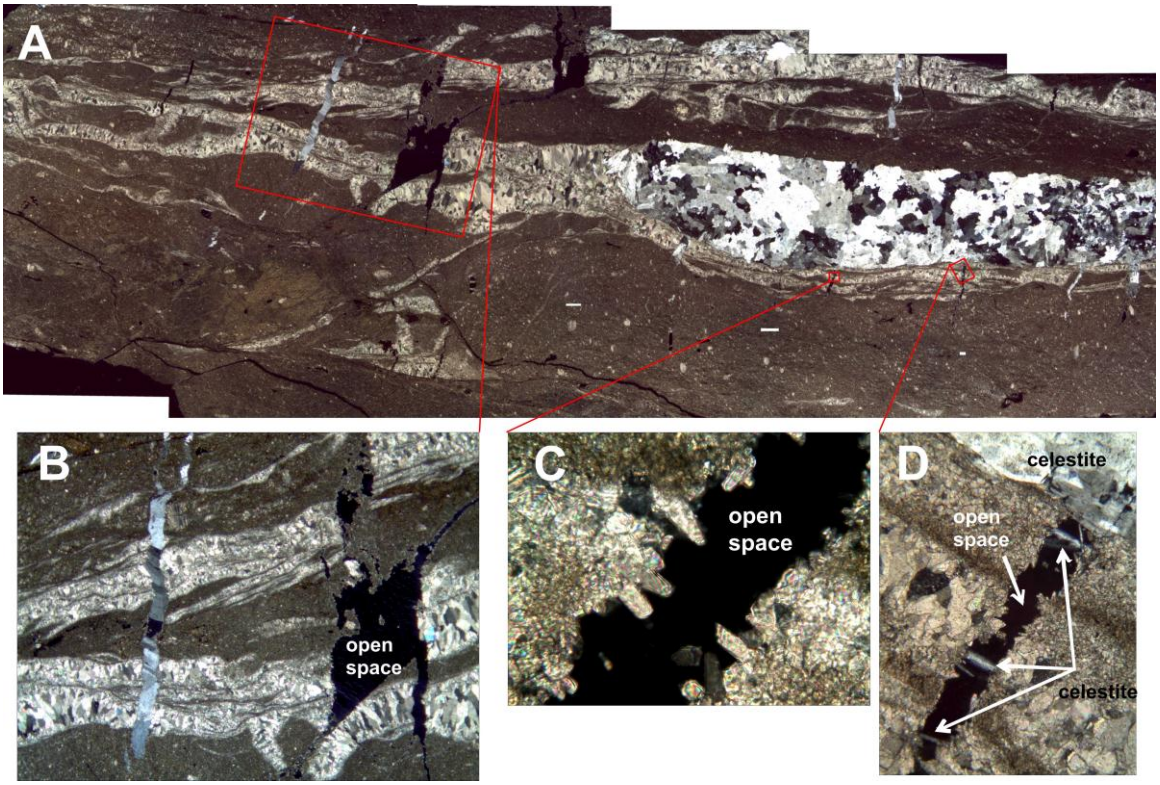

Fig. 3-3: Photomicrographs of thin section of vein in sample GM-64 (Opalinus Clay) in crossed polarized light. General view A is a composite made from 10 overlapping pictures (total width is about 3.5 cm). Length of detailed views is 7.2 mm for B, 0.36 mm for C, and 0.9 mm for D

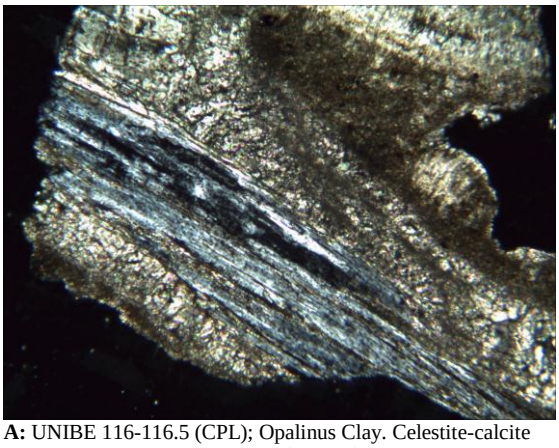

A: UNIBE 116-116.5 (CPL); Opalinus Clay. Celestite-calcite vein (see Fig. 3-2). The oriented fibres of celestite suggest syn-tectonic precipitation. Length of picture is 0.9 mm.

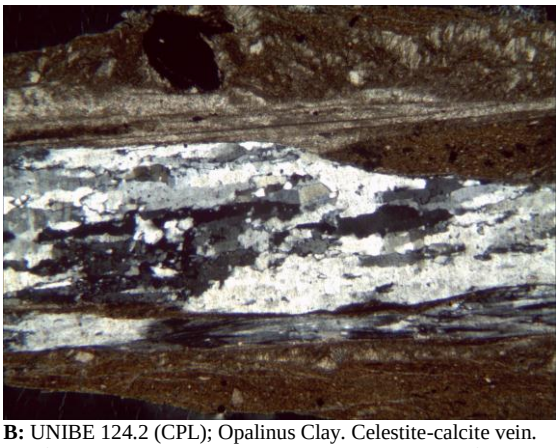

B: UNIBE 124.2 (CPL); Opalinus Clay. Celestite-calcite vein. The fibrous textures and linear patterns on both sides of the vein are evidences for syn-tectonic deposition. Length of picture is 3.5 mm.

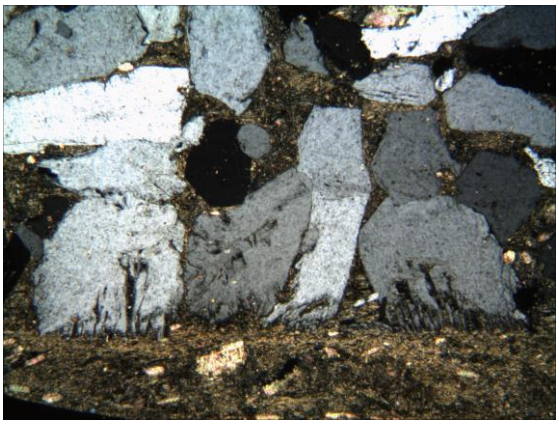

C: GM 6.8 (CPL); Opalinus Clay. Celestite vein. The contact of the vein with the host-rock is apparently tectonic (bottom of picture) and records displacement subsequent to vein formation. Length of picture is 3.5 mm.

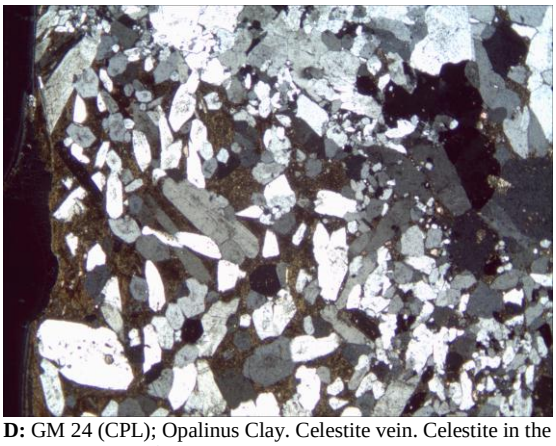

D: GM 24 (CPL); Opalinus Clay. Celestite vein. Celestite in the upper right part of the picture is massive. In contrast, in the lower part, celestite crystals are cemented by detrital clay reworked from the host-rock. The left side of the picture corresponds to a slickenside contact with the host rock. Length of picture is 7.2 mm.

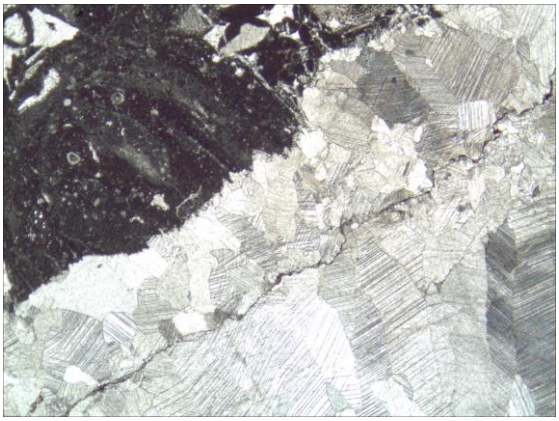

E: MT-23 (PPL); Malm kimestone. Border of a calcite vein cutting the Oolithe coralienne (Rauracian, Malm). A stylolite joint is visible in the vein calcite. Length of picture is 7.2 mm.

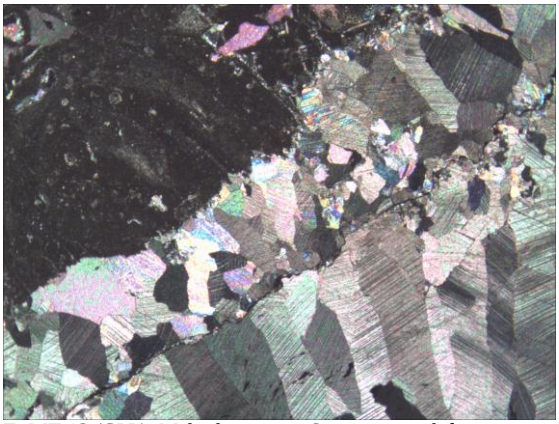

F: MT-23 (CPL); Malm limestone. Same view as left picture. Length of picture is 7.2 mm.

Fig. 3-4: Photomicrographs of thin sections of celestite-calcite (A), celestite (B to D), and calcite (E and F) veins in Opalinus Clay and Malm limestone. PPL = plane polarized light, CPL= crossed polarized light.

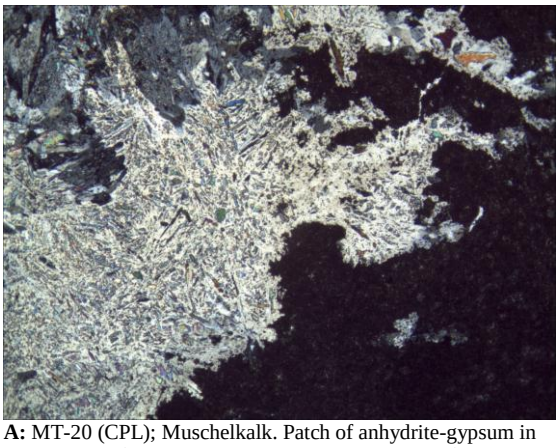

A: MT-20 (CPL); Muschelkalk. Patch of anhydrite-gypsum in Muschelkalk fine-grained dolomite (dark). Length of picture is 7.2 mm.

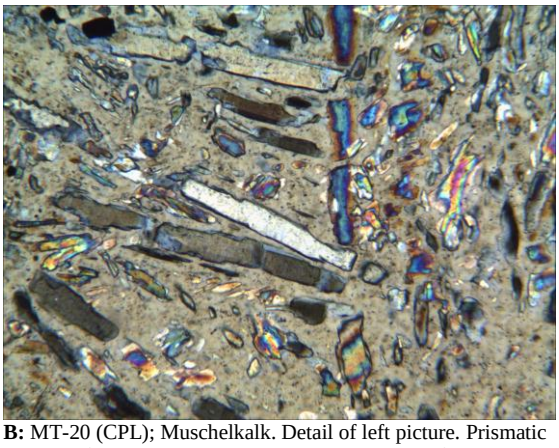

B: MT-20 (CPL); Muschelkalk. Detail of left picture. Prismatic crystals of anhydrite included in gypsum. Length of picture is 0.9 mm.

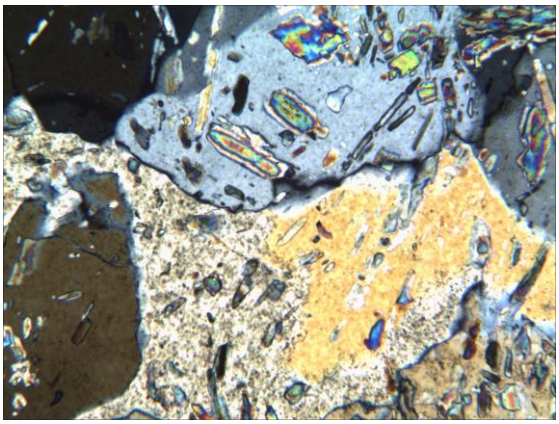

C: MT-20 (CPL); Muschelkalk. Detail of above picture. Prismatic anhydrite crystals included in larger gypsum crystals. Length of picture is 0.9 mm.

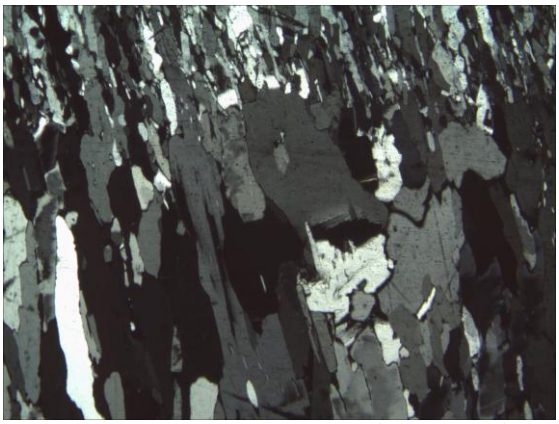

D: MT-3 (CPL); Keuper. Massive gypsum from Keuper of the "La Gypsière" outcrop, on top of the Mont Terri hill. Length of picture is 7.2 mm.

Fig. 3-5: Photomicrographs of thin sections of evaporite anhydrite (A to C) in Muschelkalk dolomite and of gypsum (D) in Keuper. Thickness of section shown in C is >30 µm, and this is why gypsum has up to first order yellow birefringence color, instead of white. CPL= crossed polarized light.

3.2 Borehole BSF-006 in the Main Fault at Mont Terri

Borehole BSF-006 was drilled in the shaly facies of Opalinus Clay, parallel to the main structures of the fault. The core includes one of the main thrust horizons. Fig. 3-6 illustrates the main structural features in cross-section. The following features can be distinguished:

- Two major and one minor horizons of fault gouge, i.e. cohesionless, fine-grained rock material along which major shear strain was accommodated. Each of the horizons is about 0.1–2 mm thick.

- The zone between the two major fault-gouge horizons (ca. 3 cm thick) consists of highly deformed rock that is crumbly and disintegrates along numerous shear bands of variable orientation if not stabilized by resin. This zone contains numerous calcite veinlets of thickness in the millimetre range. The orientation of bedding is highly disturbed, i.e. rotated and/or overprinted by tectonic fabrics.

- The rock outside the central part of the fault is deformed, although less intensely than within the fault. Calcite veins are abundant and longer (up to a few cm).

On the scale of the core cross section, the structures can be interpreted as a fault core bounded by the fault-gouge horizons and embedded in a fault-damage zone (Fig. 3.6). Note that the Main Fault contains several such zones when a larger scale is considered.

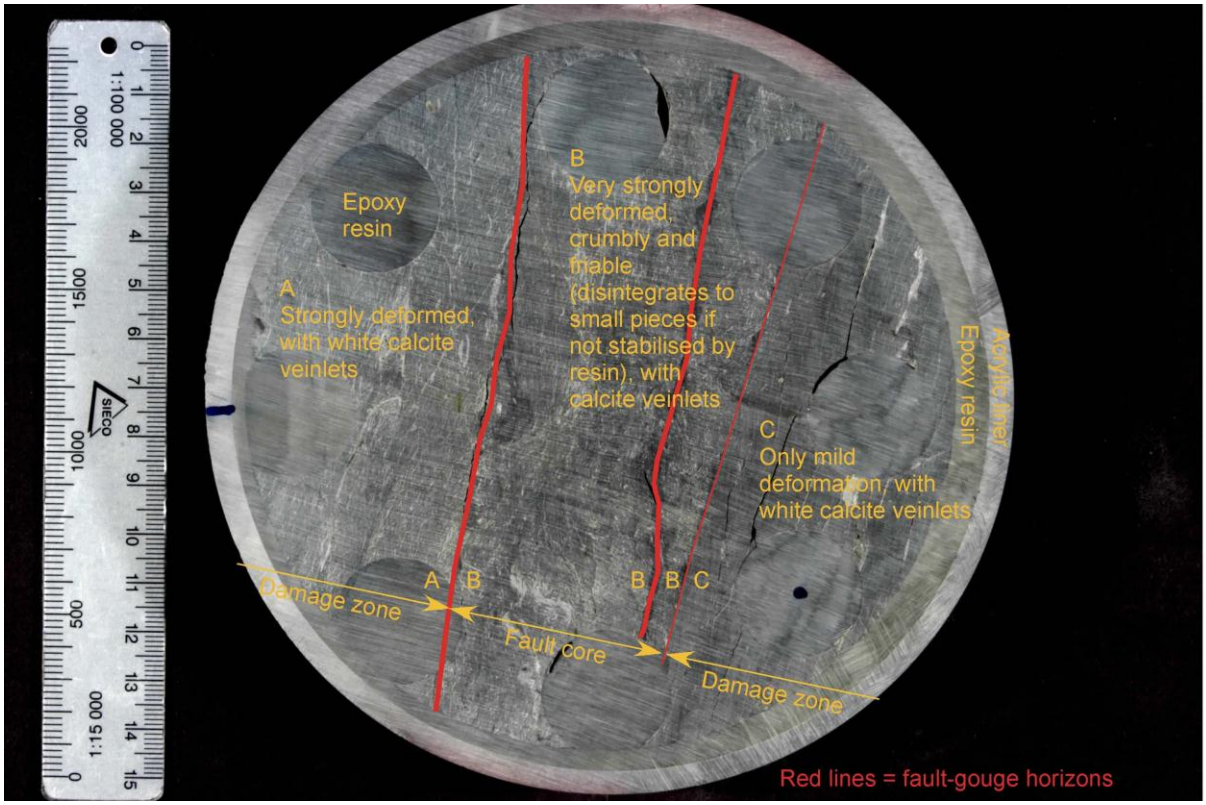

Fig. 3-6: Cross section of core BSF-006 (slice 6-17t) showing the structural elements of the penetrated fault segment

Fig. 3-7 illustrates the weakly deformed rock matrix on a microscopic scale at a distance of ca. 5 cm away from the fault core. The sample is quite clay-rich with only minor amounts of quartz. The only conspicuous heterogeneities on the cm scale are from calcite bioclasts (white) and early diagenetic pyrite (black).

The strongly deformed rock in the fault core is illustrated in Fig. 3-8. Two discrete shear bands are recognised, with connecting structures running obliquely to the orientation of the bands. The lower two thirds of the photograph show highly deformed rock in which calcite veins are disintegrated and partially recrystallized. In the upper third, a calcite vein is observed that is less strongly deformed. According to the textural interpretation, calcite precipitated syntectonically.

A fault-gouge horizon is shown in Fig. 3-9. The darker colour is likely due to the higher clay-minerals content and to the smaller average grain size. Calcite bioclasts and veinlets are comminuted to grains with sizes in the range of micrometres.

Fig. 3-7: Weakly deformed, clay-rich matrix of core BSF-006. Elongated, white structures are artificial desiccation cracks

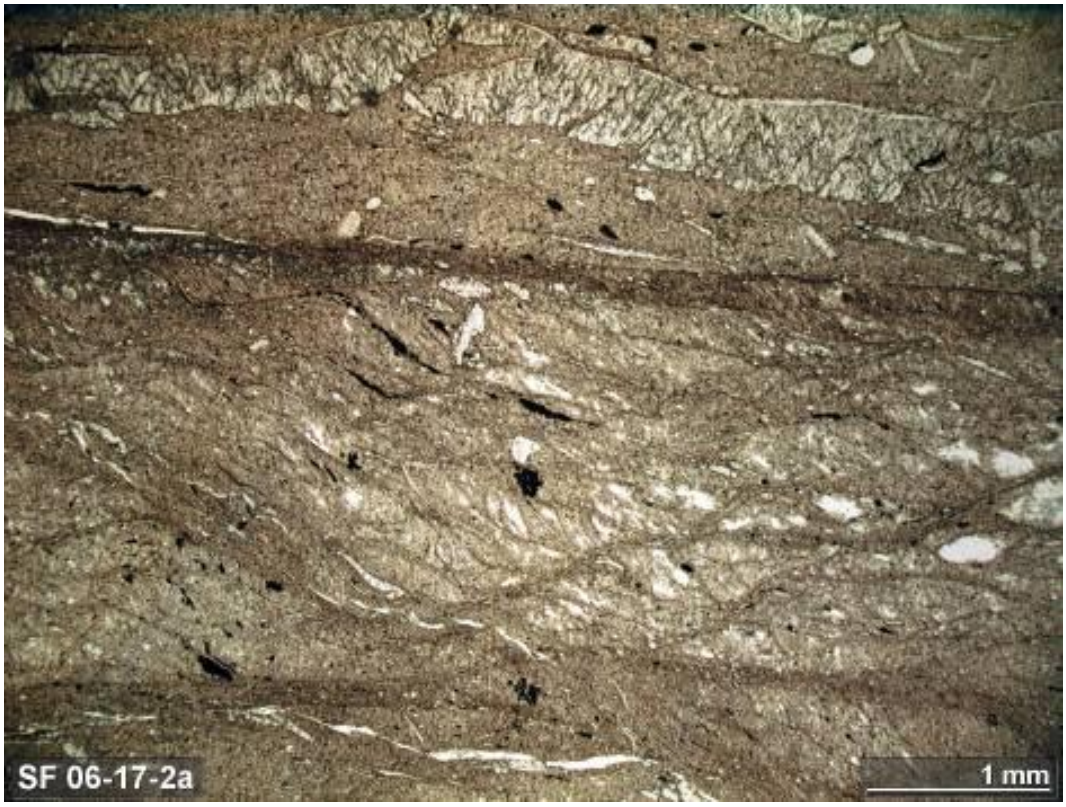

Fig. 3-8: Shear bands in the fault core

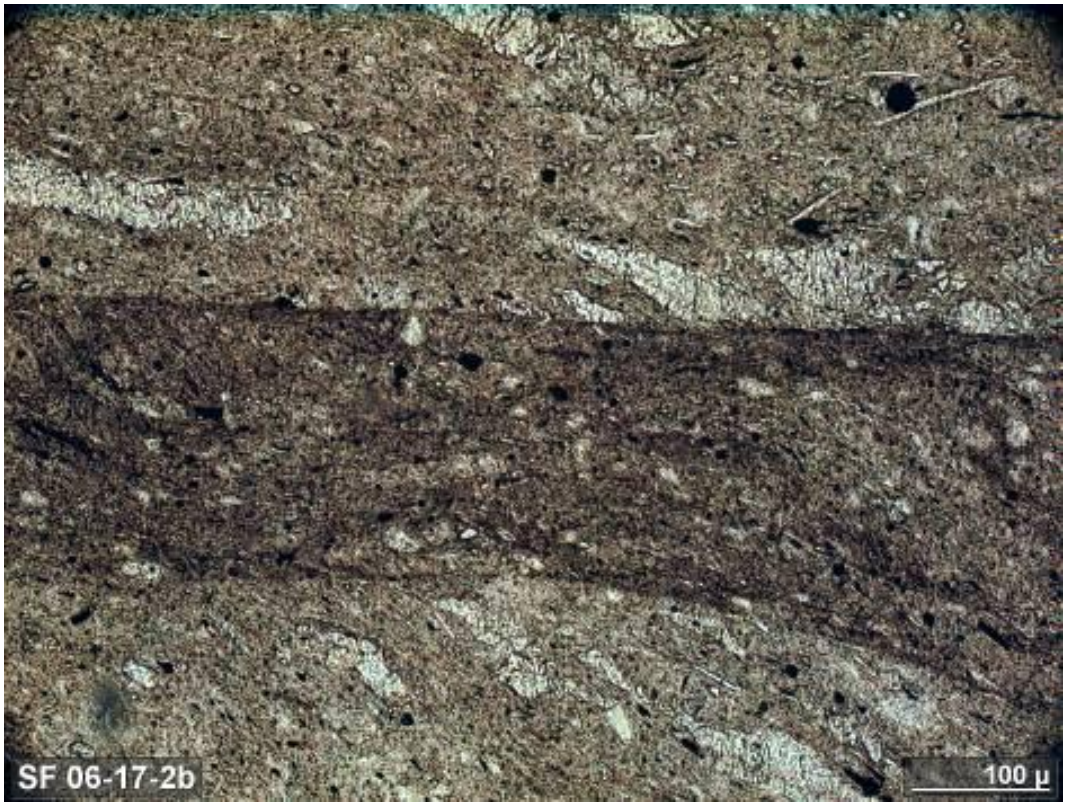

Fig. 3-9: Fault-gouge horizon

Petrographic studies using reflected-light microscopy were performed on the same rock chips used to make the covered thin sections for transmitted light petrography. Rock chips were carefully polished on one side with petrol to avoid rock disaggregation through clay swelling with water (Fig. 3-10). The purpose was to investigate the mineralogy and texture of opaque minerals present in the Opalinus Clay. The mineralogy of the opaque components identified in the investigated samples is simple and consists of pyrite, sphalerite, and carbonaceous matter. Pictures of the most typical occurrences are shown in Figs 3-11 and 3-12.

The clay-rich facies of the Opalinus Clay is relatively rich in small fossils and these are locally accumulated in thin beds (Fig. 3-11). These shell-rich beds are locally cemented by calcite, with pyrite and lesser sphalerite. The pyrite occurs as fine-grained aggregates and disseminations cemented by calcite, the grain-size being similar as framboidal pyrite (i.e. a few microns). In contrast, sphalerite tends to occur as relatively large euhedral crystals (up to ~400 µm) freely grown in the pore space between shell fragments. Aside from these shell-rich horizons, pyrite is common as very fine-grained aggregates near or within fossils (Fig. 3-12) or as isolated grains in the matrix. Carbonaceous matter grains occur disseminated in the clay-rich rock matrix.

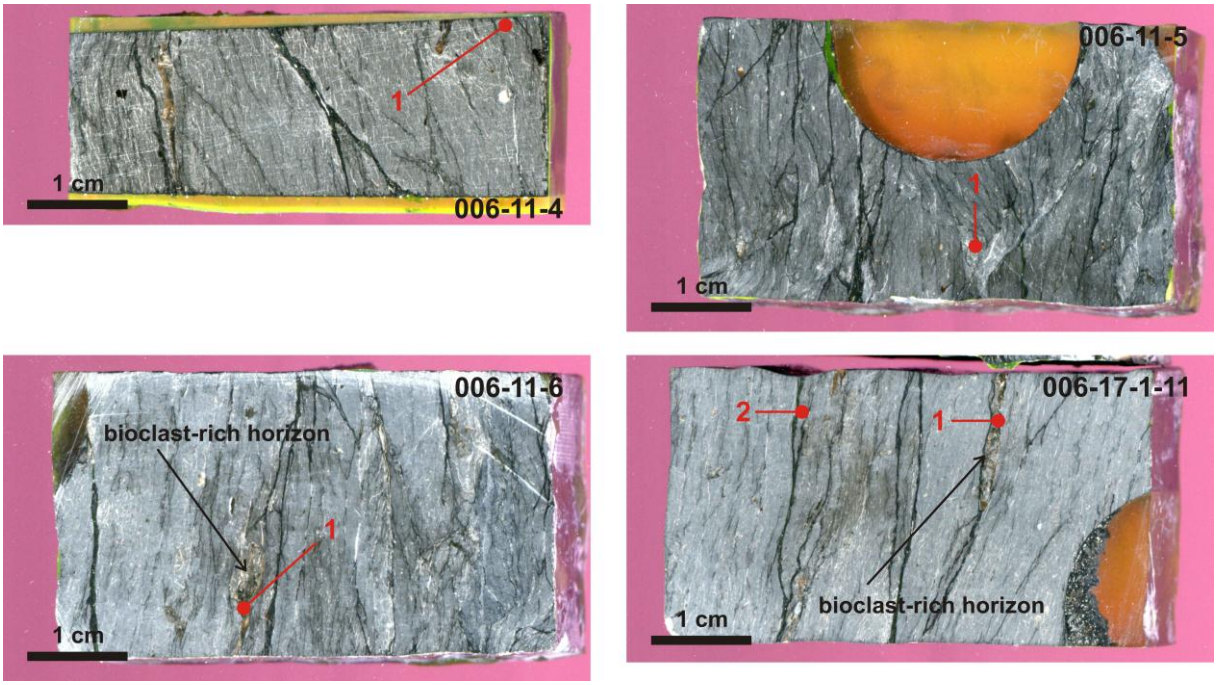

Fig. 3-10: Polished sections from the overcored borehole BSF- 006 (Main Fault). Labels of the polished sections are shown on each picture, with the first number (006) referring to the borehole, the second number to the number of the core slice, and the third to the section number. Red numbers correspond to the positions of the views shown in Figs. 3-11 and 3-12.

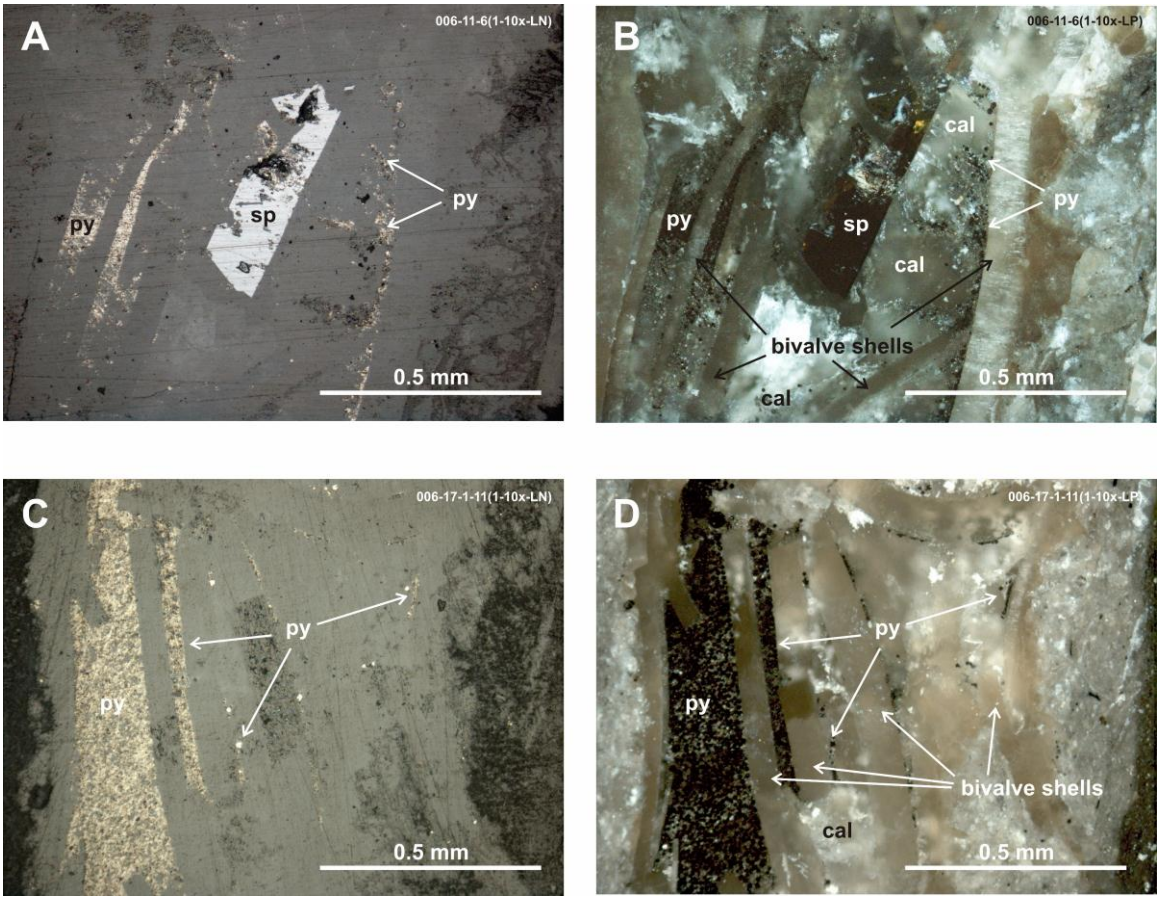

Fig. 3-11: The polished section labels (upper right corner of each picture) are completed (in parenthesis) by the number of the view (see Fig. 3-10), its magnification, and the type of light: plane-polarized (LN) or cross-polarized (LP). *A and B.* Bioclast-rich horizon with open spaces filled by microcrystalline pyrite and sphalerite, with syn- to late calcite. *C and D.* Bioclast-rich horizon with open spaces filled by microcrystalline pyrite and calcite. Abbreviations: cal = calcite, py = pyrite, sp = sphalerite.

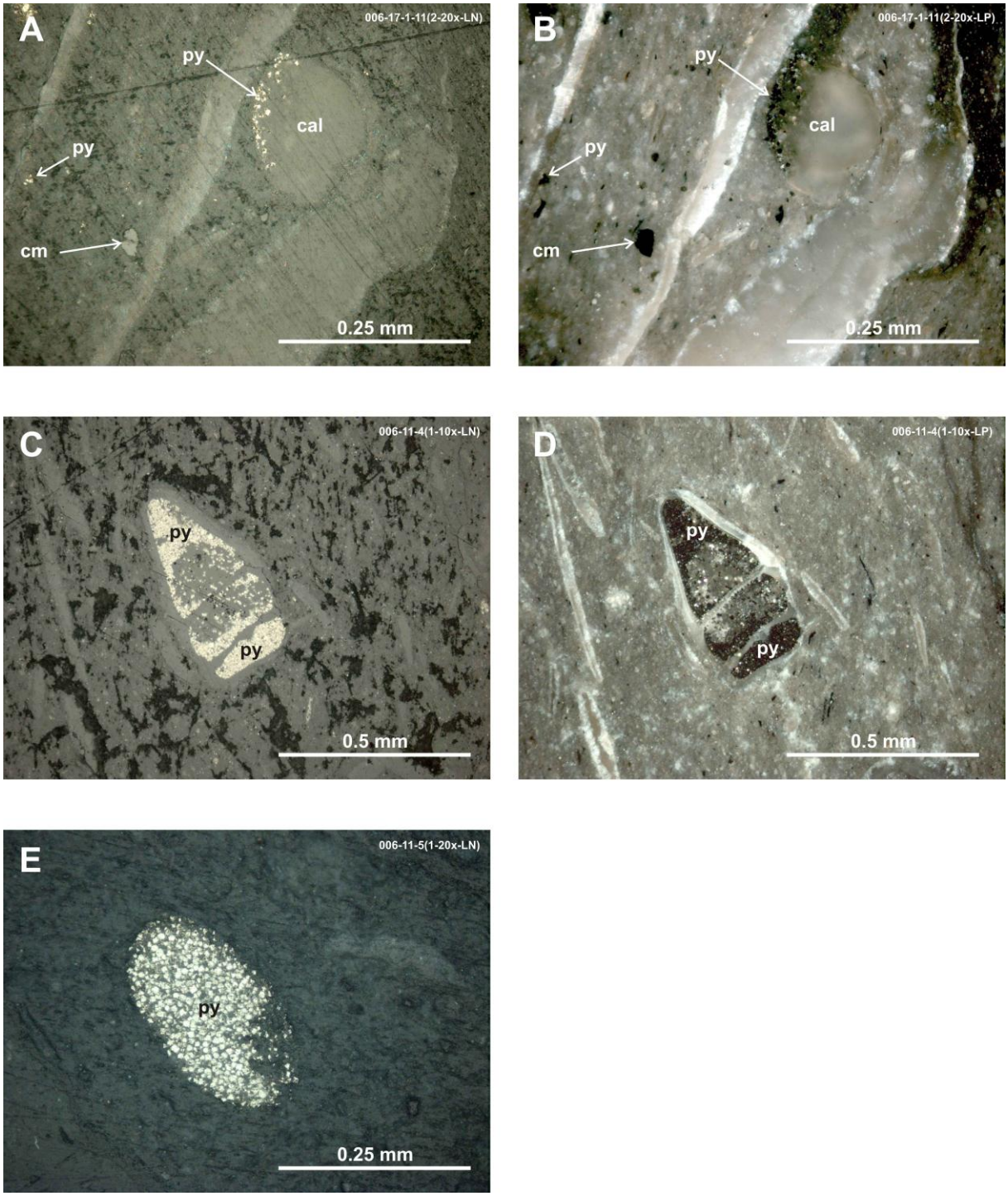

Fig. 3-12: The polished section labels (upper right corner of each picture) are completed (in parenthesis) by the number of the view (see Fig. 3-10), its magnification, and the type of light: plane-polarized (LN) or cross-polarized (LP). *A and B.* Clay-rich sediment with bioclasts (shells) and a small (~200 μm) bivalve filled with possibly diagenetic calcite and pyrite. Carbonaceous matter (vt) and pyrite grains are disseminated in the rock. *C and D.* Unidentified foraminifer filled with diagenetic microcrystalline pyrite and calcite. E. Diagenetic ovoid microcrystalline pyrite aggregate. Abbreviations: cal = calcite, cm = carbonaceous matter, py = pyrite.

3.3 Borehole BSF-004 across a celestite-calcite-bearing vein at Mont Terri

Borehole BSF-004 was drilled in the sandy facies of the Opalinus Clay and shows the presence of thin sandy layers intercalated in a clay-rich matrix. The vein that cross cuts the rock is a strictly planar feature that can be traced in the tunnel over several metres (see also Mazurek et al. 2010). It is discordant to the bedding of Opalinus Clay and is 0.2–2 cm thick (Fig. 3-13). There is no evidence of post-mineralization shear deformation.

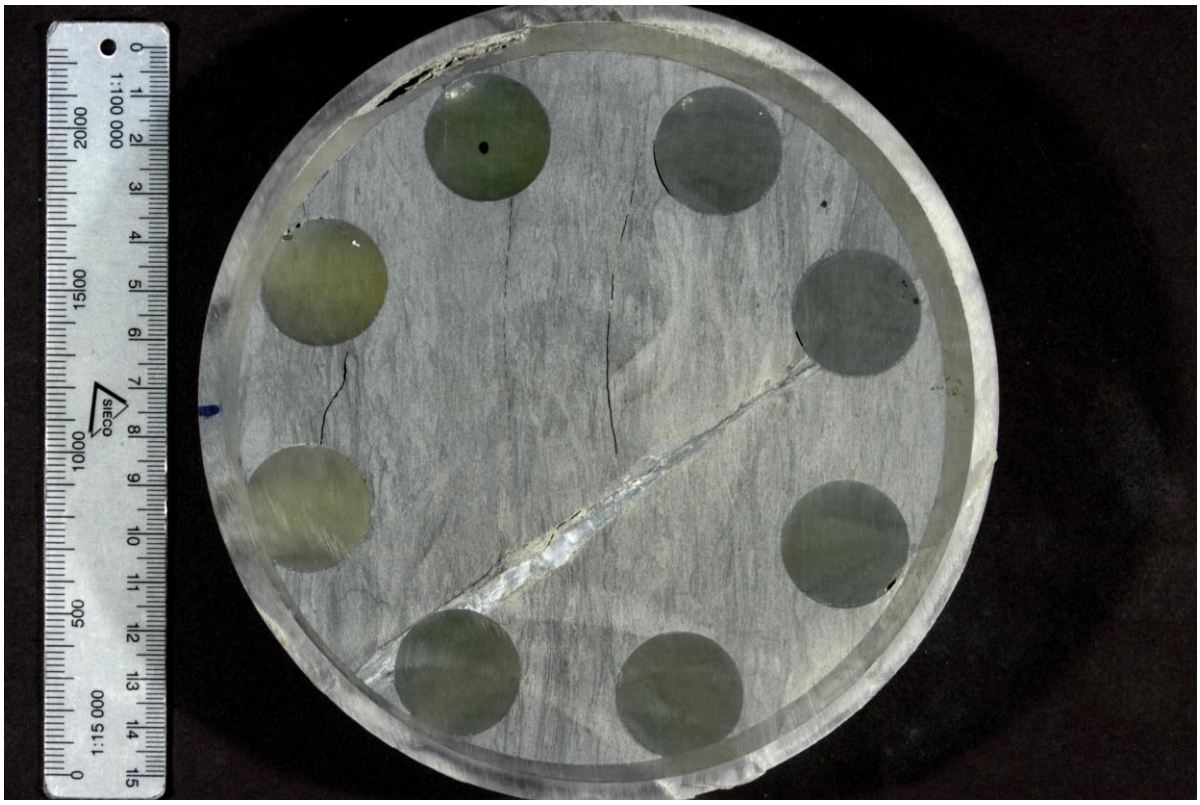

Fig. 3-13: Cross section of overcore BSF-004 (surface 4-10t) showing the celestite-calcite-bearing fracture

On a microscopic scale, a polyphase evolution of the vein becomes evident. Fig. 3-14 shows an older, deformed calcite vein (centre) and younger, weakly or undeformed celestite veins (right and left). The preferential orientation of the celestite crystals following the shear plane indicates syntectonic precipitation (right side of Fig. 3-15). Undeformed celestite needles can replace older calcite or grow into the rock matrix (Fig. 3-15).

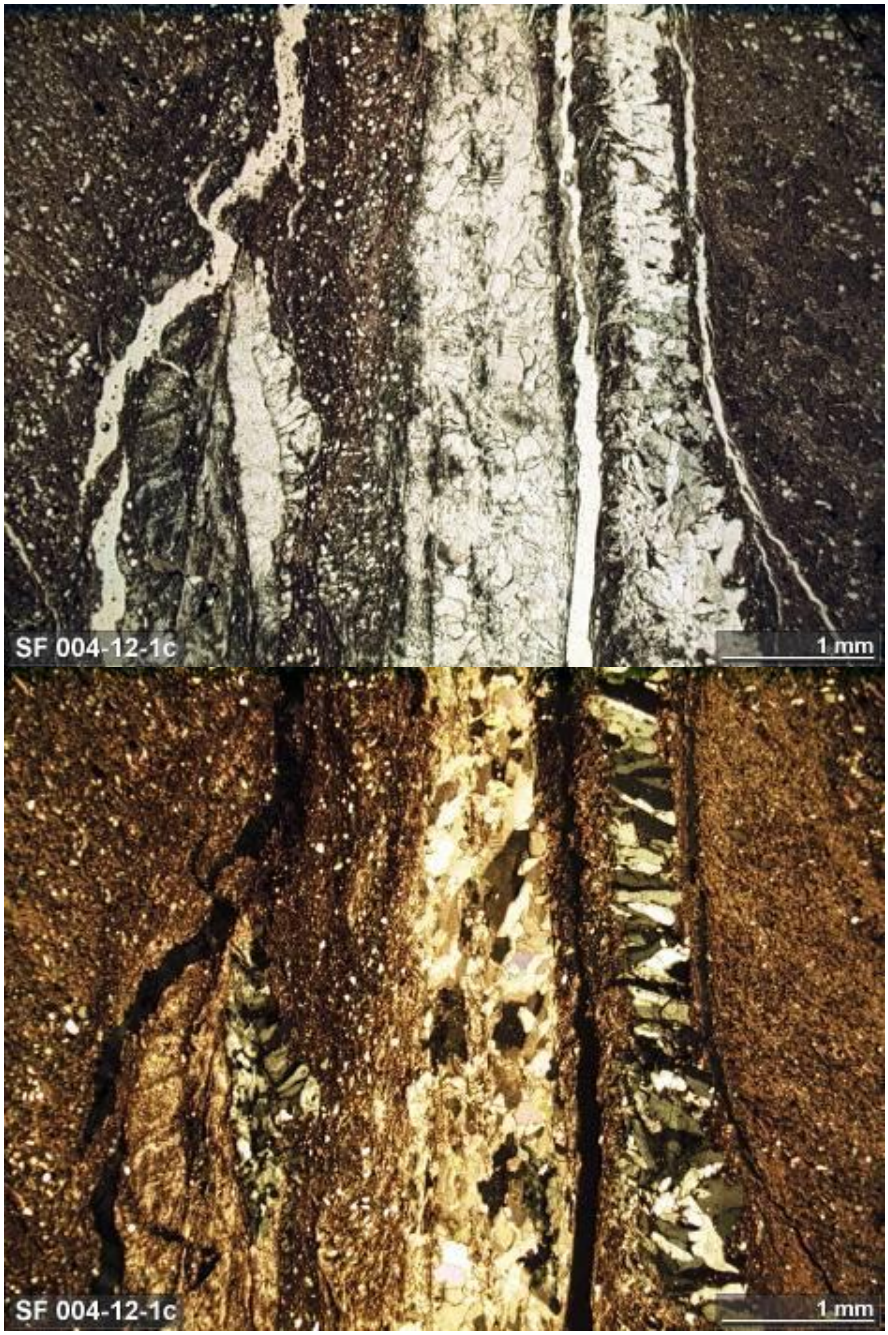

Fig. 3-14: Borehole BSF-004. Calcite (centre) and celestite veins (right and left) in Opalinus Clay. Fractures that appear white under parallel polarizers (top) and black under crossed polarizers (bottom) are artefacts of sample preparation.

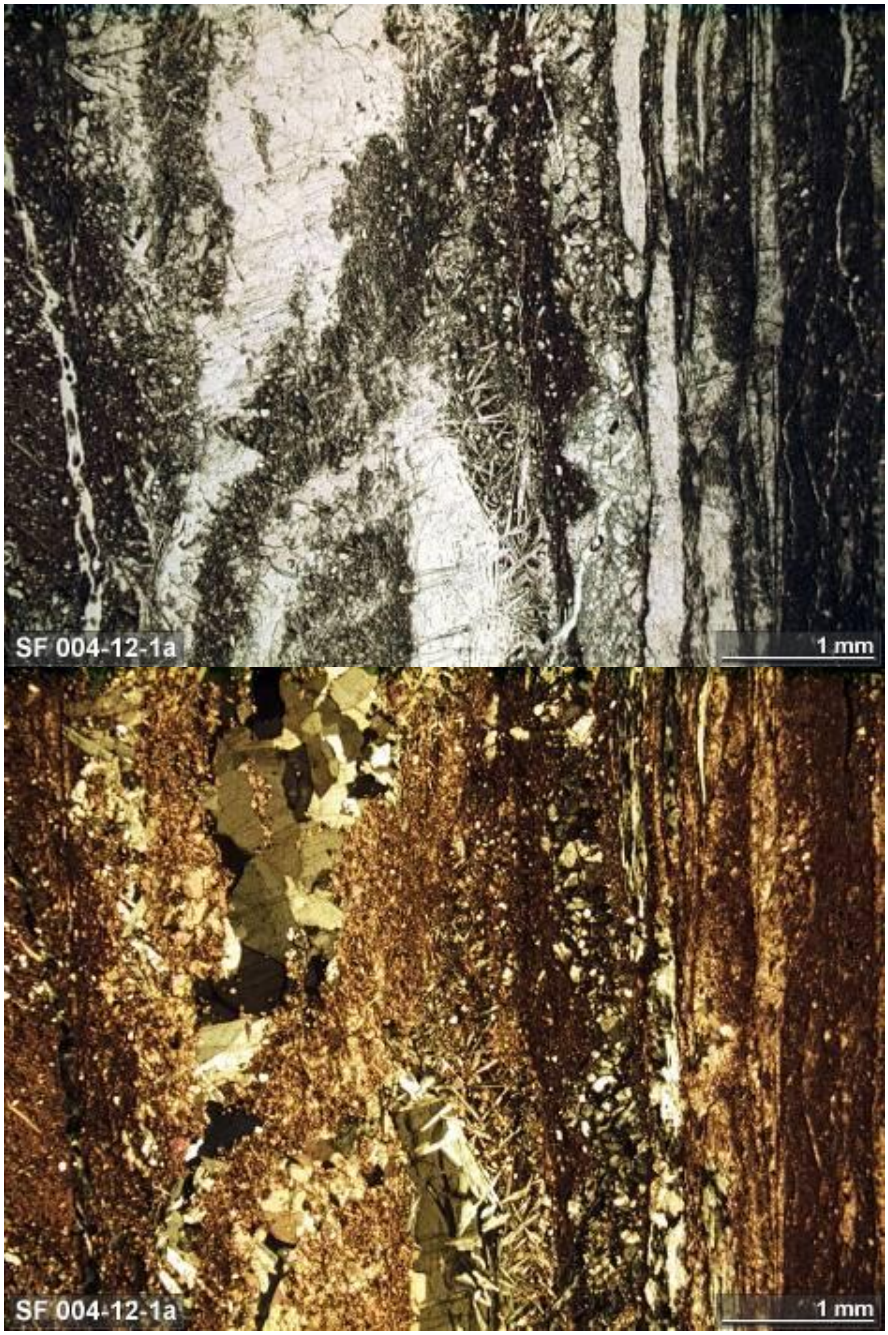

Fig. 3-15: Borehole BSF-004. Complex geometry of the vein containing older calcite with overgrowths of coarser-grained celestite. Undeformed celestite needles grown into the rock matrix in the lower central part of the illustration. The right side of the picture shows syntectonically grown calcite and celestite (fibrous) in shear planes.

According to reflected-light microscopy (overview in Fig. 3-16), the sandy layers are composed of quartz grains cemented by calcite and subordinate sulfides; mostly sphalerite, with minor pyrite (Fig. 3-17A to D and 3-18). Pyrite tends to be very fine-grained (<10 µm), while sphalerite is generally coarser (up to ~30 µm), anhedral to subhedral. The calcite cement is enclosing the sulfides and therefore postdates them. In the clay-rich matrix, pyrite occurs as framboidal aggregates, with disseminated grains of carbonaceous matter (Fig. 3-17E and F). The reflectivity of the carbonaceous matter is variable. Few grains of carbonaceous

matter associated with minor sphalerite and pyrite (Fig. 3-19A and B) were found in the calcite-celestite vein.

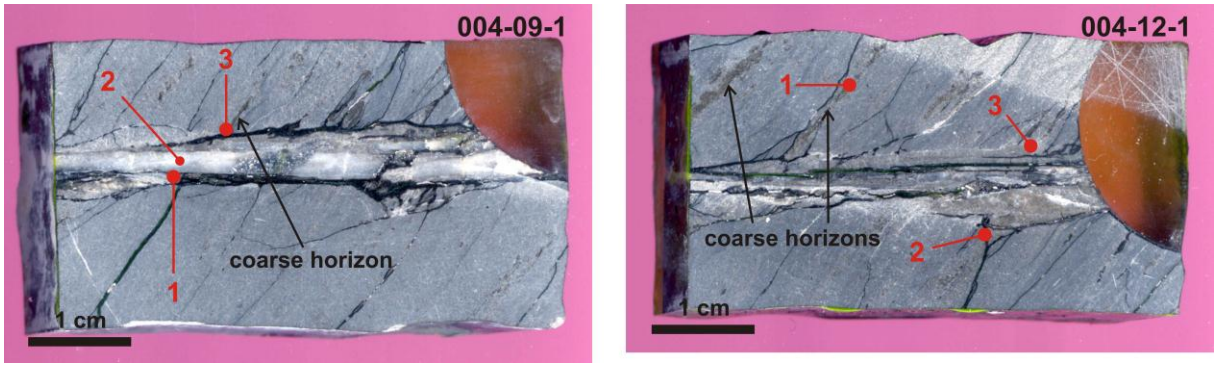

Fig. 3-16: Polished sections from the overcored borehole BSF-004 (front of GAL-04). Labels of the polished sections are shown for each picture, with the first number (e.g. 004) referring to the borehole, the second number to the distance along the borehole, and the third to the section number. Positions of the pictures shown in Figs. 3-17 and 3-18 are also given

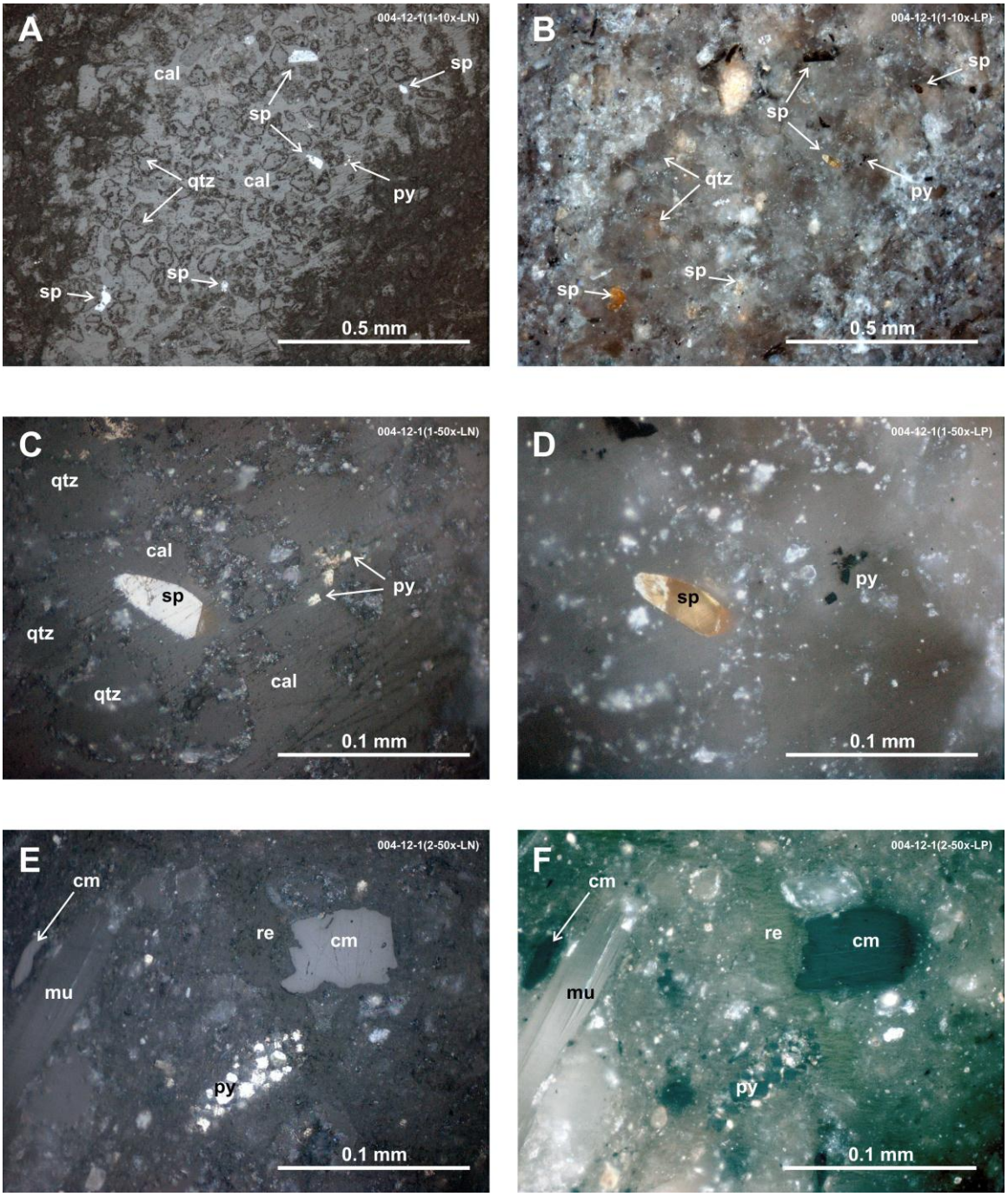

Fig. 3-17: The polished section labels (upper right corner of each picture) are completed (in parenthesis) by the number of the view (see Fig. 3-16), its magnification, and the type of light: plane-polarized (LN) or cross-polarized (LP). *A and B.* Coarse-grained quartz-rich detrital bed cemented by late calcite, sphalerite and minor pyrite.*C and D.* Detail of the view shown in A and B. *E and F.* Microgranular pyrite with carbonaceous matter grains and detrital muscovite. Abbreviations: cal = calcite, cm = carbonaceous matter, mu = muscovite, py = pyrite, qtz = quartz, sp = sphalerite.

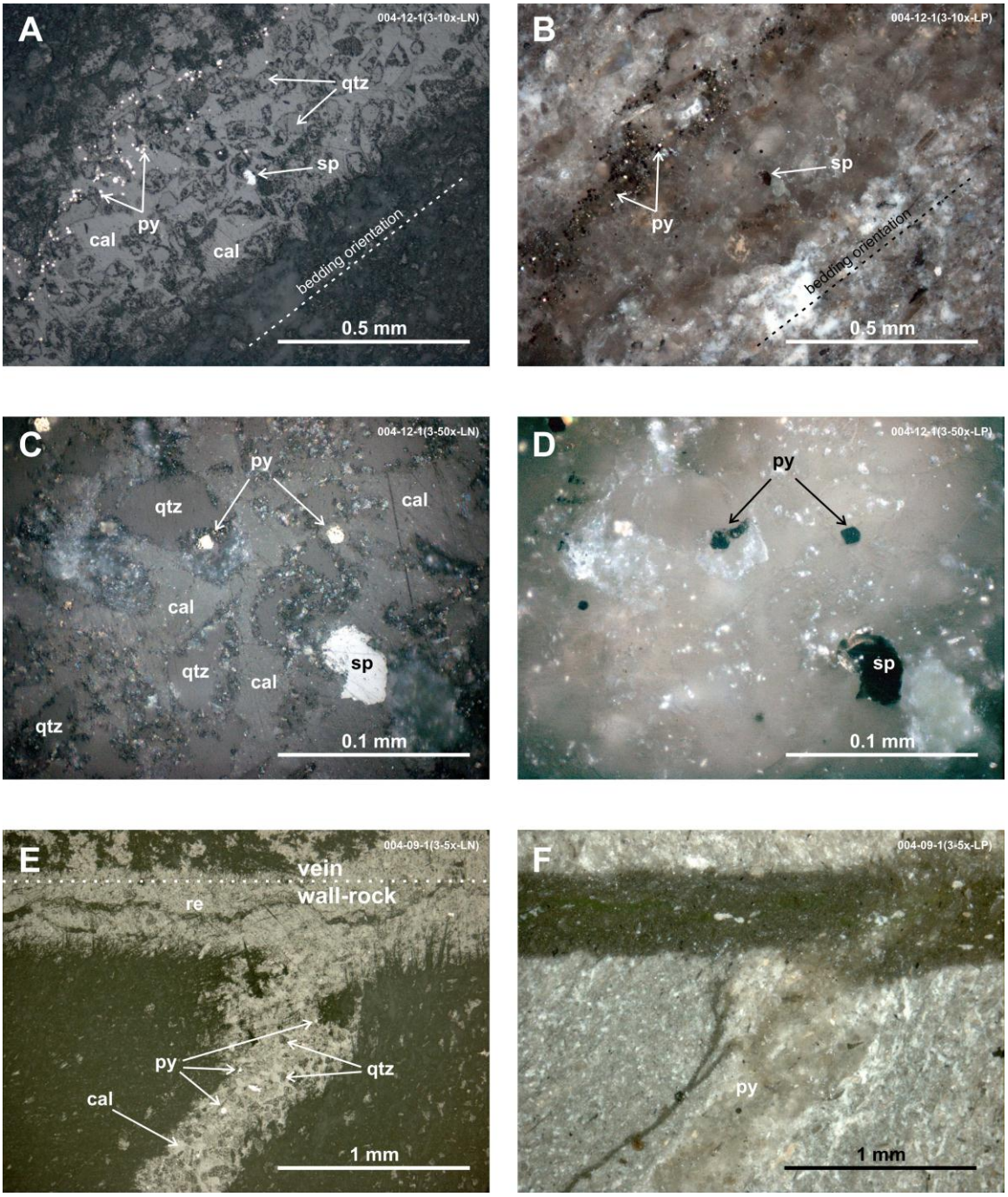

Fig. 3-18: The polished section labels (upper right corner of each picture) are completed (in parenthesis) by the number of the view (see Fig. 3-16), its magnification, and the type of light: plane-polarized (LN) or cross-polarized (LP). *A and B.* Sandy quartz-rich detrital horizon cemented by late calcite with pyrite and minor sphalerite. *C and D.* Detail of the view shown in A and B. In D, internal reflections in sphalerite are only visible on the upper left of the grain. *E and F.* Calcite (with minor pyrite) cements a sandy (quartz) horizon (~0.5 mm thick) in contact with the celestite-calcite vein. This contact is fractured (sampling artifact) and cemented by epoxy resin (re). Abbreviations: cal = calcite, py = pyrite, qtz = quartz, sp = sphalerite, and re = epoxy resin

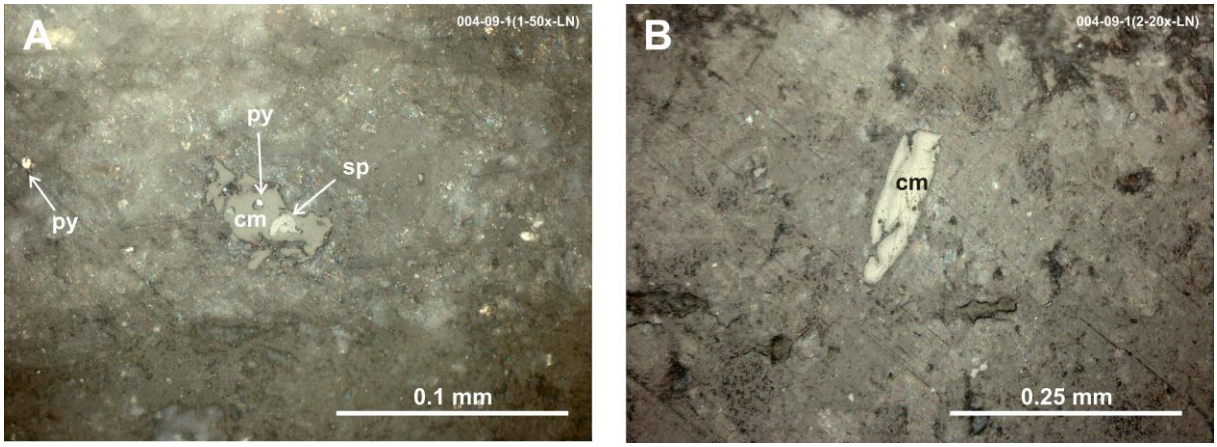

Fig. 3-19: The polished section labels (upper right corner of each picture) are completed (in parenthesis) by the number of the view (see Fig. 3-16), its magnification, and the type of light: plane-polarized (LN). *A.* Carbonaceous matter grain (~50 μm diameter) with inclusions of sphalerite and pyrite in vein. *B.* Large carbonaceous matter grain (~200 μm long) in vein. Abbreviations: cm = carbonaceous matter, py = pyrite, sp = sphalerite

3.4 BET and density measurements of BSF-004 and BSF-006 borehole subsamples

Specific surface area (BET) and density of Opalinus Clay were measured for intact, sheared and fault gouge samples. The aim was to characterize the physical property changes of the rock induced by the tectonic shear.

Results are given in Tab. 3-2 and shown in Figs. 3-20 and 3-21. They show that the intensity of shearing broadly correlates with the BET and the bulk dry density. Higher BET values correspond to fault gouge. No density measurements could be conducted on the fault gouge but sheared rock shows a tendency towards lower density than intact rock.

Tab. 3-2: Specific surface area (BET) and bulk dry density measurements on samples from boreholes BSF-004 and BSF-006

		BET			Bulk density			
Borehole	Slab #	Label	Material	BET (m^2/g)	Label	Material	Mass of sample (g)	Bulk density (g/cm^3)
BSF-004	13-14	004-(13-14)-1 M	matrix	18.003	004-(13-14)-1	matrix	19.908	2.34
		004-(13-14)-2 M	matrix	15.978	004-(13-14)-2	matrix	23.425	2.37
BSF-004	15	004-15 M	matrix	19.852	004-15	matrix	22.347	2.37
BSF-006	7-8	006-(7-8)-1 SZ	shear zone	28.396	006-(7-8)-1	shear zone	31.208	2.29
		006-(7-8)-2 SZ	shear zone	31.815	006-(7-8)-2	shear zone	22.2	2.29
		006-(7-8)-3 SZ	shear zone	32.224	006-(7-8)-3	shear zone	20.197	2.29
		006-(7-8) FG	fault gouge	37.289				
BSF-006	10	006-10-1 M	matrix	23.316	006-10-1 A	matrix	3.959	2.37
					B		4.173	2.24
		006-10-2 M	matrix	11.713	006-10-2 A	matrix	12.227	2.31
					B		7.273	2.33
		006-10-3 SZ	shear zone	19.606	006-10-3 A	shear zone	6.004	2.26
					B		3.858	2.27
BSF-006	12	006-12 SZ	shear zone	18.539	006-12 A	shear zone	12.365	2.31
					B		15.011	2.31
		006-12 FG	fault gouge	31.051				
BSF-006	13	006-13 SZ	shear zone	26.684	006-13	shear zone	26.24	2.29
		006-13 FG	fault gouge	36.454				

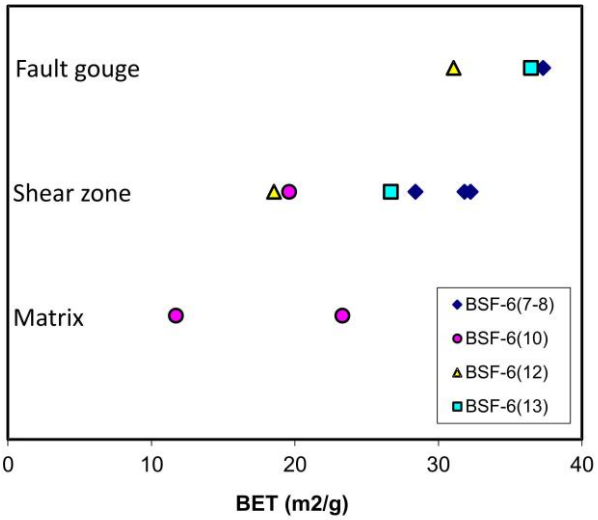

Fig. 3-20: Variation of the BET value of the rock compared with the intensity of the tectonic imprint. Matrix is for “intact” rock.

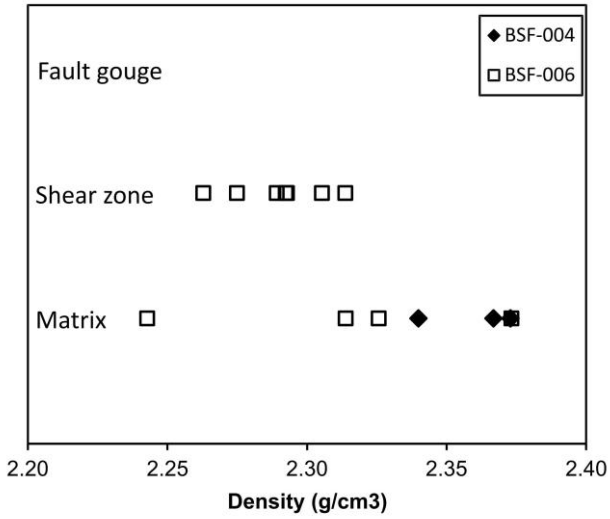

Fig. 3-21: Variation of the bulk dry density compared to the intensity of the tectonic imprint. Matrix is for “intact” rock. Density could not be measured on fault gouge samples because of the lack of cohesion.

4. Isotopic studies

4.1 Sulfur and oxygen isotopes of sulfides and sulfate minerals

Diagenetic sulfur-bearing minerals (sulfides and sulfates) were analyzed in rocks from the Trias up to the top of the Opalinus Clay, while vein celestite and pyrite were only found in the Opalinus Clay (see Tabs. 1-1 and 4-1).

Fig. 4-1 shows that $\delta^{34}S$ values from diagenetic sulfides in the rock matrix (pyrite, sphalerite, and marcasite) follow a broadly Gaussian distribution, ranging widely from -48.2 ‰ (bulk pyrite in borehole BWS-E8) to +57.8 ‰ (medium grained pyrite in borehole BWS-E6), centered at about 0 ‰. The distribution of the sphalerite values (n = 13) is apparently similar to the distribution of combined pyrite and marcasite data (n = 28 and 3, respectively). No clear systematic relationship between pyrite morphology (see section 3, and Tab. 4-1) and $\delta^{34}S$ values is evident. The distribution shown in Fig. 4-1 is for sulfides from clay-rich rocks of the Keuper-Lias boundary up to the top of the Opalinus Clay. If considering only data from the Opalinus Clay, the distribution would be similar. Also shown are the range of values for vein celestite in Opalinus Clay and for Trias evaporite (gypsum and anhydrite), and results for two pyrite samples from fibrous calcite veins. It is unclear if this pyrite is epigenetic (crystallized from vein fluids) or consists of diagenetic pyrite that has been mechanically incorporated into the calcite vein.

Fig. 4-2 shows the $\delta^{18}O$ versus $\delta^{34}S$ values of sulfate minerals from Mont Terri and Mont Russelin. It also includes data by Pearson et al. (2003) for vein celestite and barite, and porewater sulfate. Porewater sulfate data show significant perturbation between duplicate analyses that indicate redox reactions during or after sampling procedure. Oxidation of diagenetic pyrite during or before sampling possibly contributed to the sulfate content of the collected porewater, and this would have lowered the $\delta^{18}O$ and $\delta^{34}S$ values (Balci et al., 2007). Data of vein minerals and porewater sulfate are compared with the composition of evaporitic sulfate values compiled by Balderer et al. (1991). With the exception of the celestite sample from Mont Russelin (SFS-11 in Tab. 4-1), vein celestite and barite plot largely outside the Mesozoic evaporite fields and cannot be explained by direct precipitation from Jurassic seawater sulfate.

Fig. 4-3 shows the profile of sulfur isotope composition of sulfide and sulfate minerals and porewater sulfate projected along the emergency gallery metering. There is no clear trend in this profile, except that the range of sulfate $\delta^{34}S$ values is much smaller than for sulfides, which suggests a different origin, i.e. not related to early diagenesis.

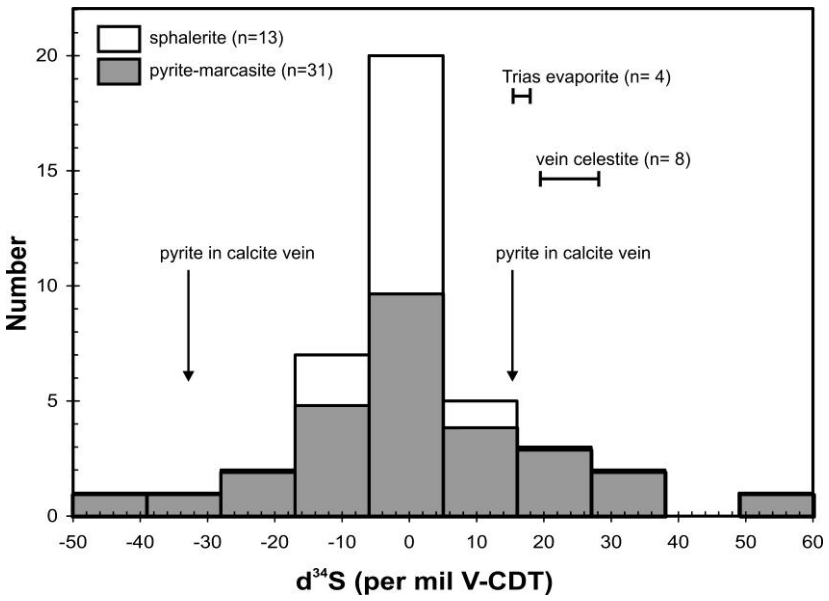

Fig. 4-1: Histogram of $\delta^{34}S$ values of diagenetic pyrite (including three values for marcasite) and sphalerite from clay-rich rocks from the Keuper-Lias boundary up to the top of the Opalinus Clay. Also indicated (but not plotted in the histogram) are the values or ranges for pyrite in calcite veins, for Trias evaporite (gypsum or anhydrite), and for vein celestite.

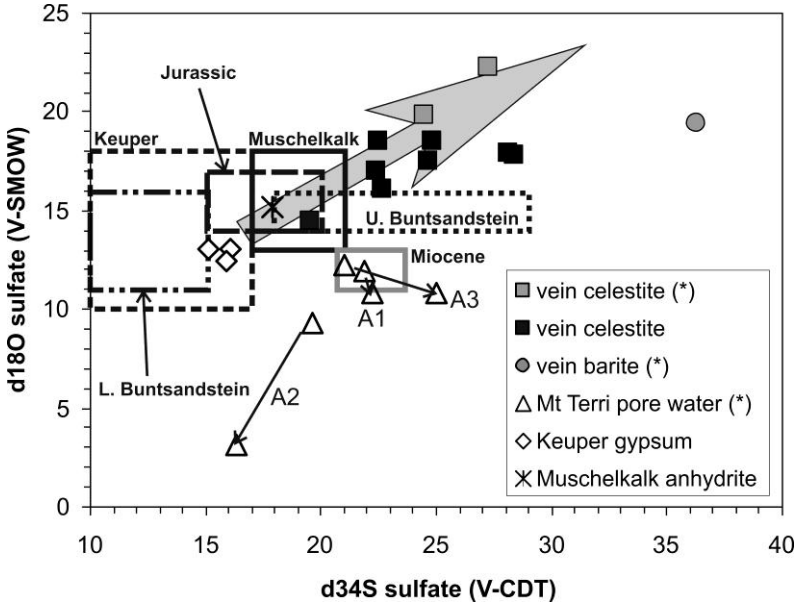

Fig. 4-2: $\delta^{18}O$ versus $\delta^{34}S$ values of mineral and porewater sulfate at Mont Terri and Mont Russelin compared to the composition ranges of evaporitic reservoirs after compilation by Balderer et al. (1991). Data labeled with (*) are from Pearson et al. (2003). The vein celestite with the lowest $\delta^{18}O$ and $\delta^{34}S$ values is from Mont Russelin. The gray arrow indicates what would be the general effect of bacterial sulfate reduction on the composition of the remaining dissolved sulfate. Labels A1 to A3 refer to sulfate in porewaters from boreholes BWS-A1 to BWS-A3 (Pearson et al. 2003). Arrows are from first to second porewater sampling, and suggest significant redox perturbations occurred during or before sampling.

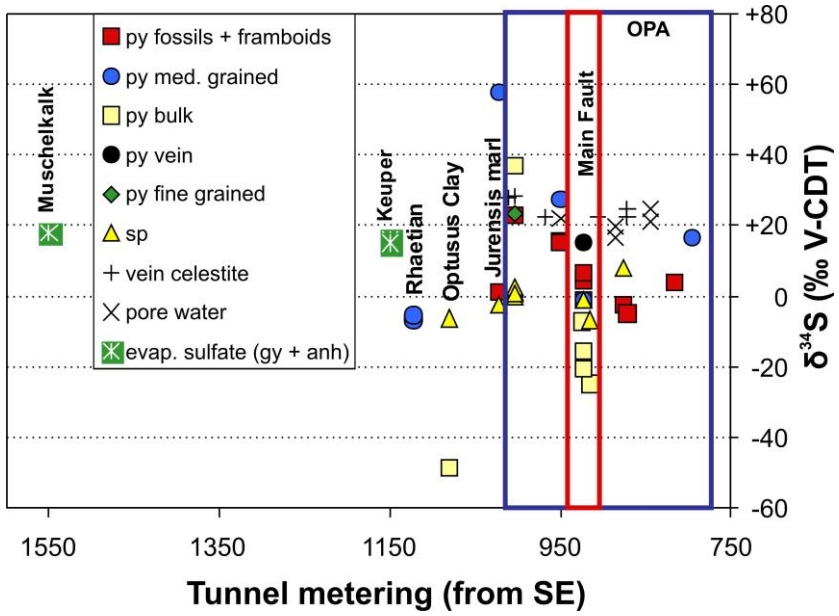

Fig. 4-3: Profile of sulfur isotope compositions of sulfide and sulfate minerals and porewater sulfate. Porewater data are from Pearson et al. (2003). All the data are projected on the emergency tunnel distance scale. Abbreviations: py = pyrite, sp = sphalerite, gy = gypsum, anh = anhydrite, evap. = evaporite. The blue box defines the boundaries of Opalinus Clay (OPA). The red box shows the Main Fault.

Tab. 4-1: Sulfur and oxygen isotopes of sulfide and sulfate minerals

Sample	Tunnel meters [1]	Sample description [2]	Diagen.	Epigen.	$\delta^{34}S_{sulfide}$ ‰ V-CDT	$\delta^{34}S_{sulfate}$ ‰ V-CDT	STD ‰ V-CDT	$\delta^{18}O_{sulfate}$ ‰ V-SMOW	STD ‰ V-SMOW
Mont Terri:									
BWS-E1(3.40-3.60)	779.4	no recoverable sulfide							
BWS-E4(3.25-3.45)	794.2	py, medium-grained aggregate	X		16.7		0.3		
BWS-E5(4.38-4.50)	814.5	py framboidal	X		3.8		0.3		
BSF-004-8	870.0	vein celestite		X		22.6	0.3	16.1	0.3
BSF-004-8	870.0	vein celestite		X		24.8	0.3	18.6	0.3
BSF-004-8	870.0	vein celestite		X		24.7	0.3	17.5	0.3
MT-9	870.0	py framboidal	X		-4.9		0.3		
BWS-A2(16.85-17.17)	875.0	py framboidal	X		-2.5		0.3		
BWS-A2(16.85-17.17)	875.0	sp crystals brownish	X		8.2		0.3		
BWS-A2(2.33-2.48)	885.2	framboidal py not recoverable (amount and grain size are too low)	X						
UNIBE-124.20	905.8	vein celestite		X		22.4	0.3	17	0.2
MT-8	915.0	py bulk (fine-grained, replaced fossils and columns)	X		-24.9		0.3		
MT-8	915.0	sp brownish crystals (5 grains)	X		-6.6		0.3		
BSF-006-(13)	923.0	py fine-grained collumns, massive	X		-20.5		0.3		
BSF-006-(13)	923.0	py replacing fossils (amm, gast)	X		6.6		0.3		
BSF-006-(7-8)	923.0	py fine-grained collumns, massive	X		-15.3		0.3		
BSF-006-(7-8)	923.0	py replacing fossils (amm, foram, gast)	X		4.3		0.3		
MT-6	923.0	sp brownish crystal (1 grains)	X		-1.3		0.3		
MT-6	923.0	py replacing fossils	X		-1.2		0.3		
MT-6	923.0	py medium-grained aggregate	X		-1.2		0.3		
MT-6	923.0	sp brownish crystals (5 grains)	X		-1.1		0.3		
MT-6	923.0	py in calcite veins (fibres)		X	15.3		0.3		
MT-7	925.0	py bulk (fine-grained, replaced fossils and columns)	X		-7.2		0.3		
BWS-A1(1.20-1.40)	949.3	py replacing fossils	X		15.2		0.3		
BWS-A1(1.20-1.40)	949.3	py replacing fossils	X		15.4		0.3		
BWS-A1(1.20-1.40)	949.3	py medium-grained, mostly collumnar	X		27.6		0.3		
GM-64	967.0	vein celestite		X		22.5	0.2	18.5	0.3
GM-24	1003.0	vein celestite		X		28.4	0.4	17.8	1.4
BWS-A6(19.55-19.75)	1003.5	sp (brownish crystals and fossils	X		-0.1		0.3		
BWS-A6(19.55-19.75)	1003.5	sp (brownish crystals and fossils	X		0.7		0.3		
BWS-A6(19.55-19.75)	1003.5	sp (brownish crystals and fossils	X		0.9		0.3		
BWS-A6(19.55-19.75)	1003.5	sp (brownish crystals and fossils	X		1.3		0.3		
BWS-A6(19.55-19.75)	1003.5	sp (brownish crystals and fossils	X		2.0		0.3		
BWS-A6(19.55-19.75)	1003.5	sp (brownish crystals and fossils	X		2.6		0.3		

[1] samples are sorted according to their location projected on the security gallery metering (0 m at SE entrance).

[2] Abbreviations: py = pyrite, sp = sphalerite, mc = marcasite, gyp = gypsum, ahn = anhydrite, Amm = ammonite, foram = foraminifer, gast = gasteropod

Tab. 4-1 (cont.)

Sample	Tunnel meters [1]	Sample description [2]	Diagen.	Epigen.	$\delta^{34}S_{sulfide}$ ‰ V-CDT	$\delta^{34}S_{sulfate}$ ‰ V-CDT	STD ‰ V-CDT	$\delta^{18}O_{sulfate}$ ‰ V-SMOW	STD ‰ V-SMOW
Mont Terri:									
BWS-A6(19.55-19.75)	1003.5	py framboidal	X		22.9		0.3		
BWS-A6(19.55-19.75)	1003.5	py fine-grained flat	X		23.3		0.3		
BWS-A6(19.55-19.75)	1003.5	py bulk	X		36.7		0.3		
GM-6.8	1010.0	vein celestite		X		28.1	0.4	17.9	0.5
BWS-E6(5.00-5.15)	1022.1	sp brownish to brown crystals	X		-2.3		0.3		
BWS-E6(5.00-5.15)	1022.1	sp brownish to brown crystals	X		-2.3		0.3		
BWS-E6(5.00-5.15)	1022.1	py fossils (amm, foram, gast)	X		1.4		0.3		
BWS-E6(5.00-5.15)	1022.1	py, medium-grained aggregate	X		57.8		0.3		
BWS-E7(4.95-5.10)	1050.6	no recoverable sulfide							
BWS-E8(4.70-5.10)	1080.4	py bulk (fine to medium-grained, massive and columns)	X		-48.2		0.3		
BWS-E8(4.70-5.10)	1080.4	sp brownish to brown crystals	X		-6.1		0.3		
BWS-E9(4.80-5.10)	1121.9	mc single coarse aggregate	X		-6.5		0.3		
BWS-E9(4.80-5.10)	1121.9	mc bulk (coarse-grained)	X		-6.4		0.3		
BWS-E9(4.80-5.10)	1121.9	py(mc?) medium-	X		-6.0		0.3		
BWS-E9(4.80-5.10)	1121.9	mc single coarse aggregate	X		-5.3		0.3		
MT-3	*1150.0*	evaporite gypsum (microdrilled)	X			16.1	0.3	13.0	0.4
MT-3	*1150.0*	evaporite gypsum (microdrilled)	X			15.9	0.3	12.5	0.4
MT-3	*1150.0*	evaporite gypsum (microdrilled)	X			15.2	0.3	13.0	0.4
MT-20	1550.0	evaporite anh/gyp	X			17.9	0.3	15.2	0.4
Mont Russelin:									
MR-SF7		py replacing	X		15.2		0.3		
		py fine-grained flat	X		-29.9		0.3		
		py fine-grained	X		3.6		0.3		
		py in calcite vein		X	-32.9		0.3		
SFS-11		celestite-calcite veins		X		19.5	1.3	14.5	2

[1] samples are sorted according to their location projected on the security gallery metering (0 m at SE entrance). Values in ***italics*** are tentative (projection from surface outcrop).

[2] Abbreviations: py = pyrite, sp = sphalerite, mc = marcasite, gyp = gypsum, ahn = anhydrite, Amm = ammonite, foram = foraminifer, gast = gasteropod

4.2 Oxygen and carbon isotopes of carbonate minerals, and strontium isotopes of carbonate and sulfate minerals

Stable oxygen and carbon isotope compositions and strontium isotopic ratios of carbonate minerals in whole rock or veins and strontium isotopes of sulfate minerals in evaporite and veins have been analyzed on samples from the geochemical profile of gallery 08 (G08) and from the large profile ranging from the Trias to the Malm (Tab. 4-2). Data of the small geochemical profile are presented first, followed by the large profile.

Results from the G08 gallery profile are shown in Fig. 4-4. The $\delta^{18}O$ values of whole rock carbonate plot at about 24-25 per mil V-SMOW, while vein calcite shows lower values, ranging from about 19 to 21 per mil V-SMOW (Fig. 4-4A). The data for echinoderm

fragments are similar to whole-rock carbonate, but small bivalve fragments have a lower value, between whole-rock carbonate and vein calcite. These bivalve fragments show a diagenetic calcite overgrowth on their surface. The $\delta^{13}C$ values of carbonate (Fig. 4-4B) range from about -2.5 to -0.5 per mil V-PDB and are less clearly differentiated than $\delta^{18}O$, although with a tendency towards lower values for vein calcite compared to whole-rock carbonate or fossil fragments. A broad correlation exists between the $\delta^{18}O$ and $\delta^{13}C$ values (Fig. 4-4C). Echinoderm fragments show the highest $\delta^{13}C$ value, although not very different from the small bivalve fragments, while whole rock carbonate values are slightly lower. No clear difference is observed in the $\delta^{18}O$ and $\delta^{13}C$ values of whole-rock carbonate within or outside the Main Fault.

The gallery G08 $^{87}Sr/^{86}Sr$ profile of carbonate and sulfate minerals is plotted in Fig. 4-4D. Vein minerals (calcite and celestite) show a nearly constant $^{87}Sr/^{86}Sr$ value. In contrast, values for whole-rock carbonate samples are more dispersed and tend to be higher than vein minerals. Fossil fragments, on the contrary, plot at lower values, the echinoderm value fitting well with the seawater Sr composition at the time of deposition (Aalenian) of the Opalinus Clay (McArthur et al. 2001). The small bivalve debris plots at an intermediate position between primary seawater and vein minerals, in agreement with what observed for $\delta^{18}O$ and $\delta^{13}C$. Plots of the $^{87}Sr/^{86}Sr$ ratio versus $\delta^{13}C$ or $\delta^{18}O$ value are shown in Fig. 4-4E and F.

The data of the large isotope profile ranging from the Trias to the Malm also include those of the G08 gallery profile and are plotted in Fig. 4-5. Results for $\delta^{18}O$ values (Fig. 4-5A) fit with those of the small profile, with the highest values for whole-rock carbonate and the lowest for the vein calcite, in particular within or close to the Main Fault. A weak shift toward lower $\delta^{18}O$ values of the whole-rock carbonate fraction of the Opalinus Clay within and near the Main Fault is visible but might not be significant. The $\delta^{13}C$ values (Fig. 4-5B) show a much clearer distribution than in the restricted G08 gallery profile (Fig. 4-5B), with most of the whole-rock carbonate plotting between -0.5 and +3 per mil V-PDP, except within or close to the Main Fault, where values tend to approach those of vein calcite, at around -2 per mil. Vein calcite shows decreasing $\delta^{13}C$ values going upward from the base of the Opalinus Clay (+0.56‰ V-PDB) to the Malm (-7.15 ‰ V-PDB), but data are highly clustered near the Main Fault in the Opalinus Clay, and more samples would be necessary to really define a trend. The whole-rock carbonate $\delta^{13}C$ value of sample BWS-E9 (boundary between Rhaetian and Gryphaea limestone; black shale and limestone) at 1150 m in the profile is anomalously negative compared to the rest of the profile. Because the shale fraction of this sample is rich in organic matter full of biogenic marcasite, it might be that this negative $\delta^{13}C$ value relates to the intense diagenetic bacterial sulfate reduction required to produce sulfides.

The large $^{87}Sr/^{86}Sr$ whole-rock carbonate profile (Fig. 4-5C) shows low values for the Malm, then increasing downward in the Dogger and attaining a plateau in the Opalinus Clay down to the Muschelkalk. The values obtained for the Malm and the Trias are in relatively good agreement with those of McArthur et al. (2001) for contemporary seawater, but the $^{87}Sr/^{86}Sr$ ratio in the Dogger to the Keuper interval is higher. This correlates with higher clay content. This enrichment is apparently related to a contribution from Sr adsorbed on the clay or from dissolution of Sr-bearing silicate minerals (feldspar and clay) having a higher $^{87}Sr/^{86}Sr$ ratio than the carbonate. Lerouge et al. (2010) documented that up to about 50% of the Sr contribution in an acetic acid leach is from strontium adsorbed on clay minerals and not from carbonate. Therefore, the whole-rock carbonate data obtained from samples from the Dogger down to the basis of the Jurassic might reflect a mixture between the seawater Sr at the time of deposition (extracted from carbonate) and the Sr adsorbed on clays (if excluding dissolution of silicate minerals). The sorbed Sr should be at equilibrium (same isotope ratio)

with the porewater Sr. However, published Sr data (at around 0.7077) of porewater collected from boreholes BWS-A1 to A3 (Pearson et al. 2003) show lower ratios than the values obtained for whole rock carbonate in this study ($^{87}Sr/^{86}Sr$ around 0.708). It follows that such low values for the present day porewater Sr would not explain the higher ratio obtained on the whole rock carbonate fraction, and might suggest acetic leach releases some radiogenic Sr from the siliciclastic minerals by dissolution. Therefore, the whole-rock carbonate data obtained from clay-rich samples from the Dogger down to the base of the Jurassic probably reflect a mixture between the seawater Sr at the time of deposition (extracted from carbonate), the Sr adsorbed on clays, and probably some Sr released by clay or feldspar minerals dissolution during the acetic acid leach and from the porewater. Implication is that the standard acetic acid leach is able to characterize the Sr isotopic composition of a fluid at equilibrium with a limestone, a dolostone, or an evaporite sulfate (gypsum or anhydrite) but not if the rock is rich in clay minerals. More work is needed to better understand the Sr contributors during acetic acid leach of clay-rich rocks.

In the profile, the whole-rock carbonate Sr ratio from samples close or within the Main Fault show some poorly defined lowering compared to the rest of the profile in the Opalinus Clay, down to values close to vein minerals, which could suggest some perturbation. However, because of the just discussed poor understanding of the whole-rock Sr isotope results from clay-rich rocks, this observation is not considered to be relevant at this stage. In contrast with the whole-rock Sr data, the $^{87}Sr/^{86}Sr$ ratio of vein minerals (calcite and celestite) from Malm and Opalinus Clay are remarkably constant, at around 0.7077.

Fig. 4-6 shows the relationship between the $^{87}Sr/^{86}Sr$ ratio and the $\delta^{18}O$ of sulfate in vein celestite, evaporite gypsum and anhydrite, and porewater sampled in the Opalinus Clay (Pearson et al. 2003). All the data are within the range of $^{87}Sr/^{86}Sr$ ratio published for Keuper seawater (McArthur et al. 2001). As mentioned before, the $\delta^{18}O$ values of the porewater sulfate are apparently significantly perturbed by redox reactions and real values might be much higher than measured if diagenetic pyrite oxidation occurred during or before sampling. The vein celestite data show a very good correlation along a mixing line broadly connecting the Trias evaporite field with a reservoir characterized by slightly lower $^{87}Sr/^{86}Sr$ ratio and higher sulfate $\delta^{18}O$ value. The $^{87}Sr/^{86}Sr$ values of celestite are similar to the range of values obtained from vein calcite. In contrast to the $^{87}Sr/^{86}Sr$ ratio versus sulfate $\delta^{18}O$ relationship, there is no correlation between the sulfate $\delta^{34}S$ value and the $^{87}Sr/^{86}Sr$ ratio of the vein celestite samples.

Tab. 4-2: Carbon, oxygen, and strontium isotope data

Sample	Tunnel meters [1]	Lithostratigraphic Unit	Rock	Sample description	Sr ppm	$^{87}Sr/^{86}Sr$	2STD	$\delta^{13}C_{CO3}$ ‰ V-PDB	STD ‰ V-PDB	$\delta^{18}O_{CO3}$ ‰ V-SMOW	STD ‰ V-SMOW
Mont Terri: Whole rock carbonate (Sr data: 0.5 M acetic acid leach)											
MT-25	35.0	Oolithe coralienne	Oolithic limestone	whole rock carbonate		0.707094	0.000027	0.41	0.05	24.52	0.06
MT-24	255.0	Oolithe coralienne	Oolithic limestone cut by minor calcite veins.	whole rock carbonate		0.70709	0.000021	0.63	0.05	24.91	0.06
MT-21	675.0	Hauptrogenstein (Oolithe	Oolithic limestone	whole rock carbonate		0.707203	0.00002	2.99	0.05	25.99	0.06
MT-22	725.0	Blaukalk	Sandy-argillaceous limestone	whole rock carbonate		0.707427	0.000021	1.21	0.05	24.24	0.06
BWS-E1(3.40-3.60)	779.4	Lower Dogger	Shale	whole rock carbonate		0.707628	0.00003	-0.16	0.05	24.87	0.06
BWS-E4(3.25-3.45)	794.2	Opalinus Clay	Shale	whole rock carbonate		0.708012	0.000032	-0.09	0.05	25.04	0.06
BWS-E5(4.38-4.50)	814.5	Opalinus Clay	Shale	whole rock carbonate		0.707842	0.000026	0.46	0.05	25.73	0.06
BWS-A3(28.00-28.12)	843.5	Opalinus Clay	Shale	whole rock carbonate		0.707986	0.000025	2.34	0.05	29.06	0.06
MT-9	870.0	Opalinus Clay	Shale	whole rock carbonate		0.70801	0.000026	-0.29	0.05	25.33	0.06
BWS-A2(2.33-2.48)	885.2	Opalinus Clay	Shale	whole rock carbonate		0.708187	0.000024	0.2	0.05	24.15	0.06
UNIBE-119.75	910.3	Opalinus Clay	Shale	whole rock carbonate		0.707806	0.000023	-1.01	0.05	24.26	0.06
UNIBE-118.25	911.8	Opalinus Clay	Shale	bioclastic calcite: echinoderm		0.70733	0.000034	-0.68	0.05	24.73	0.06
UNIBE-118.25	911.8	Opalinus Clay	Shale	bioclastic calcite: white bivalve shells		0.707555	0.000036	-0.96	0.05	22.1	0.06
UNIBE-118.75	911.3	Opalinus Clay	Shale	whole rock carbonate		0.707925	0.00002	-1.27	0.05	24.99	0.06
UNIBE-114.75	915.3	Opalinus Clay	Shale	whole rock carbonate		0.708038	0.000027	-1.58	0.05	24.95	0.06
MT-7	925.0	Opalinus Clay	Shale	whole rock carbonate		0.707847	0.000025	-1.35	0.05	23.43	0.06
BWS-A6(19.55-19.75)	1003.5	Opalinus Clay	Shale	whole rock carbonate		0.708147	0.000032	0.08	0.05	26.06	0.06
BWS-E6(5.00-5.15)	1022.1	Jurensis Marl	Shale	whole rock carbonate		0.707957	0.000034	0.28	0.05	24.93	0.06

[1] samples are sorted according to their location projected on the security gallery metering (0 m at SE entrance).

Tab. 4-2 (cont.)

Sample	Tunnel meters [1]	Lithostratigraphic Unit	Rock	Sample description	Sr ppm	$^{87}Sr/^{86}Sr$	2STD	$\delta^{13}C_{CO3}$ ‰ V-PDB	STD ‰ V-PDB	$\delta^{18}O_{CO3}$ ‰ V-SMOW	STD ‰ V-SMOW
Mont Terri: Whole rock carbonate (Sr data: 0.5 M acetic acid leach)											
BWS-E7(4.95-5.10)	1050.6	Posidonia Shale	Bituminous shale	whole rock carbonate		0.707225	0.000026	1.12	0.05	24.57	0.06
BWS-E8(4.70-5.10)	1080.4	Obtusus Clay & Obliqua layer	Shale	whole rock carbonate		0.707819	0.000037	0.13	0.05	27.7	0.06
BWS-E9(4.80-5.10)	1121.9	Rhaetian / Gryphaea limestone	limestone fraction	whole rock carbonate	270	0.707762	0.000023				
BWS-E9(4.80-5.10)	1121.9	Rhaetian / Gryphaea limestone	shale fraction	whole rock carbonate	2378	0.708433	0.000036				
BWS-E9(4.80-5.10)	1121.9	Rhaetian / Gryphaea limestone	Limestone + shale	whole rock carbonate		0.708757	0.000032	-3.18	0.05	26.84	0.06
MT-3	*1150.0*	Rhaetian	Evaporite gypsum	evaporite gypsum		0.707932	0.00003				
MT-20	1550.0	Trigonodus-Dolomite	Bedded dolomite (anhydrite-gypsum)	whole rock carbonate		0.707984	0.000033	0.89	0.05	29.14	0.06
Mt Terri: Vein material (Sr data: 0.5M acetic acid leach if calcite, HNO_3 leach if celestite)											
MT-23	275.0	Oolithe coralienne	calcite veins	vein calcite		0.707768	0.000038	-7.15	0.05	21.64	0.06
BSF-004-8	870.0	Opalinus Clay	Shale	vein celestite		0.707759	0.000022				
UNIBE-124.20	905.8	Opalinus Clay	Shale	vein calcite-		0.707749	0.000022	-2.08	0.05	19.32	0.06
UNIBE-123.5	906.5	Opalinus Clay	Shale	vein calcite		0.707764	0.000022	-2.29	0.05	21.07	0.06
UNIBE-118.25	911.8	Opalinus Clay	Shale	vein calcite		0.707796	0.000028	-1.85	0.05	19.91	0.06
UNIBE-116.25	913.8	Opalinus Clay	Shale	vein calcite (+celestite?)		0.707776	0.000037	-1.84	0.05	19.34	0.06
UNIBE-113.75	916.3	Opalinus Clay	Shale	vein calcite		0.707701	0.000026	-2.37	0.05	19.96	0.06
BSF-006-(13)	923.0	Opalinus Clay	Shale	vein calcite		0.707848	0.000026	-2.12	0.05	19.59	0.06
MT-6	923.0	Opalinus Clay	Shale	vein calcite		0.707783	0.000024	-2.05	0.05	19.88	0.06
GM-64	967.0	Opalinus Clay	Shale	vein celestite		0.707712	0.00002				
GM-24	1003.0	Opalinus Clay	Shale	vein celestite		0.707725	0.000028				
GM-6.8	1010.0	Opalinus Clay	Shale	vein calcite-		0.707726	0.000024	0.56	0.05	22.87	0.06
Mont Russelin: Vein material (Sr data: 0.5M acetic leach for calcite)											
MR-SF7		Opalinus Clay	Shale	vein calcite-		0.707853	0.000022	-0.36	0.05	17.11	0.06
BSF11 (13-15)		Opalinus Clay	Shale	calcite-celestite		0.707804	0.000023	-0.28	0.05	17.39	0.06

[1] samples are sorted according to their location projected on the security gallery metering (0 m at SE entrance). Value in ***italics*** is tentative (projection from surface outcrop).

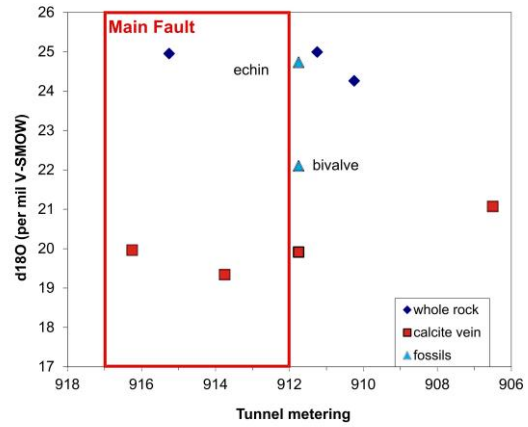

A. Tunnel profile of $\delta^{18}O$ values. The position of the Main Fault is shown with a red box.

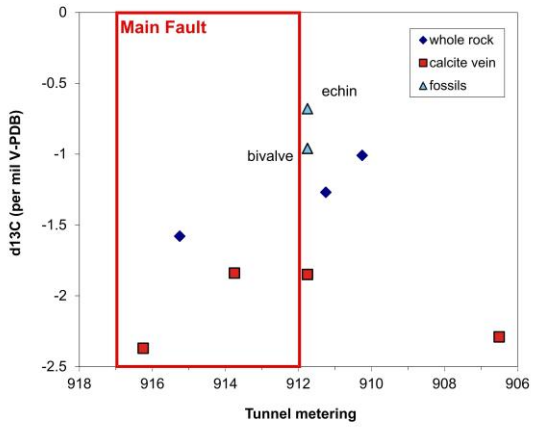

B. Tunnel profile of $\delta^{13}C$ values. The position of the Main Fault is shown with a red box.

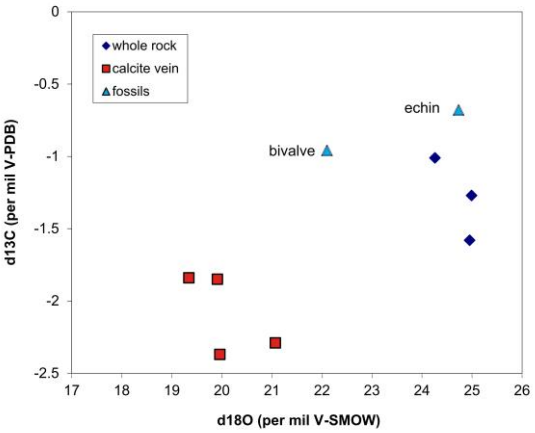

C. $\delta^{13}C$ versus $\delta^{18}O$ values of whole rock carbonate, vein calcite and fossils.

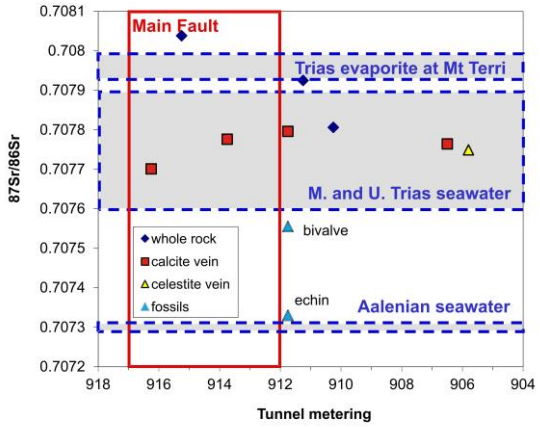

D. Tunnel profile of $^{87}Sr/^{86}Sr$ ratio. The position of the Main Fault is shown with a red box. Dashed grey boxes show Sr isotopic composition of selected seawaters and evaporite.

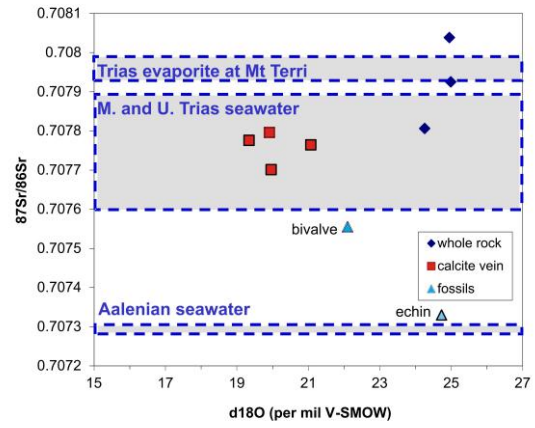

E. $^{87}Sr/^{86}Sr$ ratio versus $\delta^{18}O$ value. Dashed grey boxes show Sr isotopic composition of selected seawaters and evaporite.

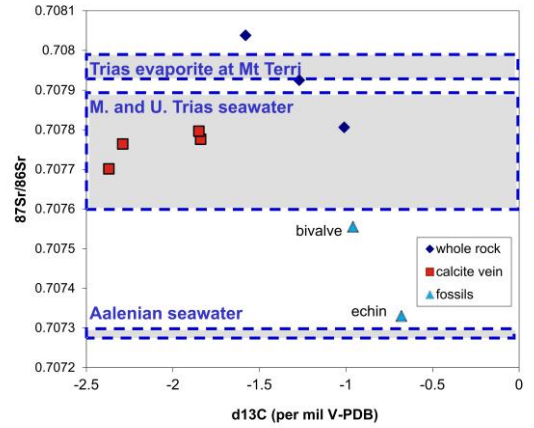

F. $^{87}Sr/^{86}Sr$ ratio versus $\delta^{18}O$ value. Dashed grey boxes show Sr isotopic composition of selected seawaters and evaporite.

Fig. 4-4: Oxygen, carbon, and strontium isotope data from the geochemical profile in Opalinus Clay of Gallery 08. Whole rock label relates to whole rock carbonate (acetic acid digestion). Two analyses of fossils have been included: one of echinoderm and one of bivalve shell fragments.

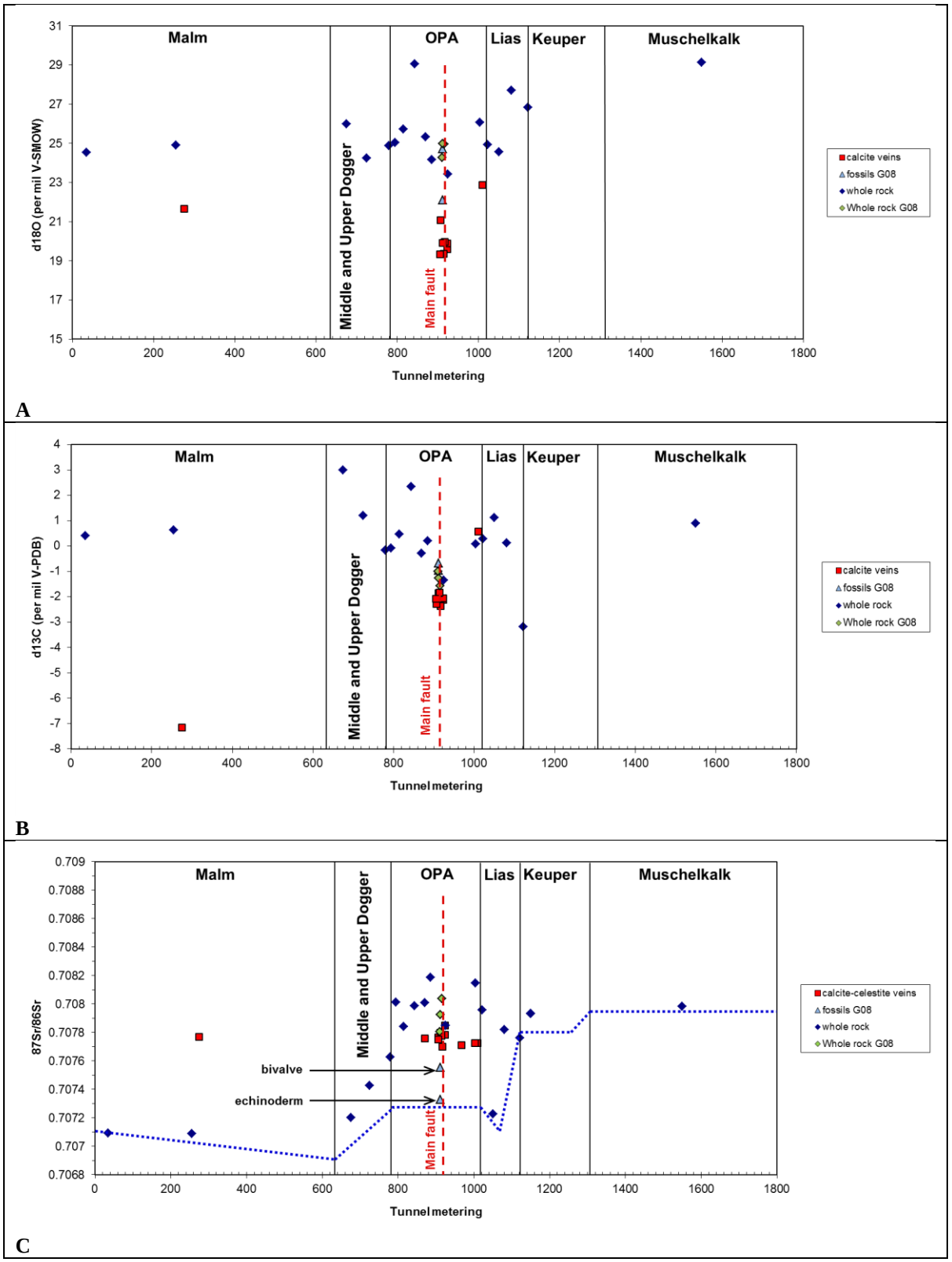

Fig. 4-5: Tunnel profiles for O, C, and Sr isotope data, looking towards SE. The red dashed line shows the position of the Main Fault. A: Tunnel profile of the $\delta^{18}O$ value of calcite veins, fossils, and whole rock carbonate. B: Tunnel profile of the $\delta^{13}C$ value of calcite veins, fossils, and whole rock carbonate. C: Tunnel profile of the $^{87}Sr/^{86}Sr$ ratio of calcite-celestite veins, fossils, and whole rock carbonate. The dotted blue line approximates the Sr composition of seawater at the time of sedimentation (McArthur et al., 2001).

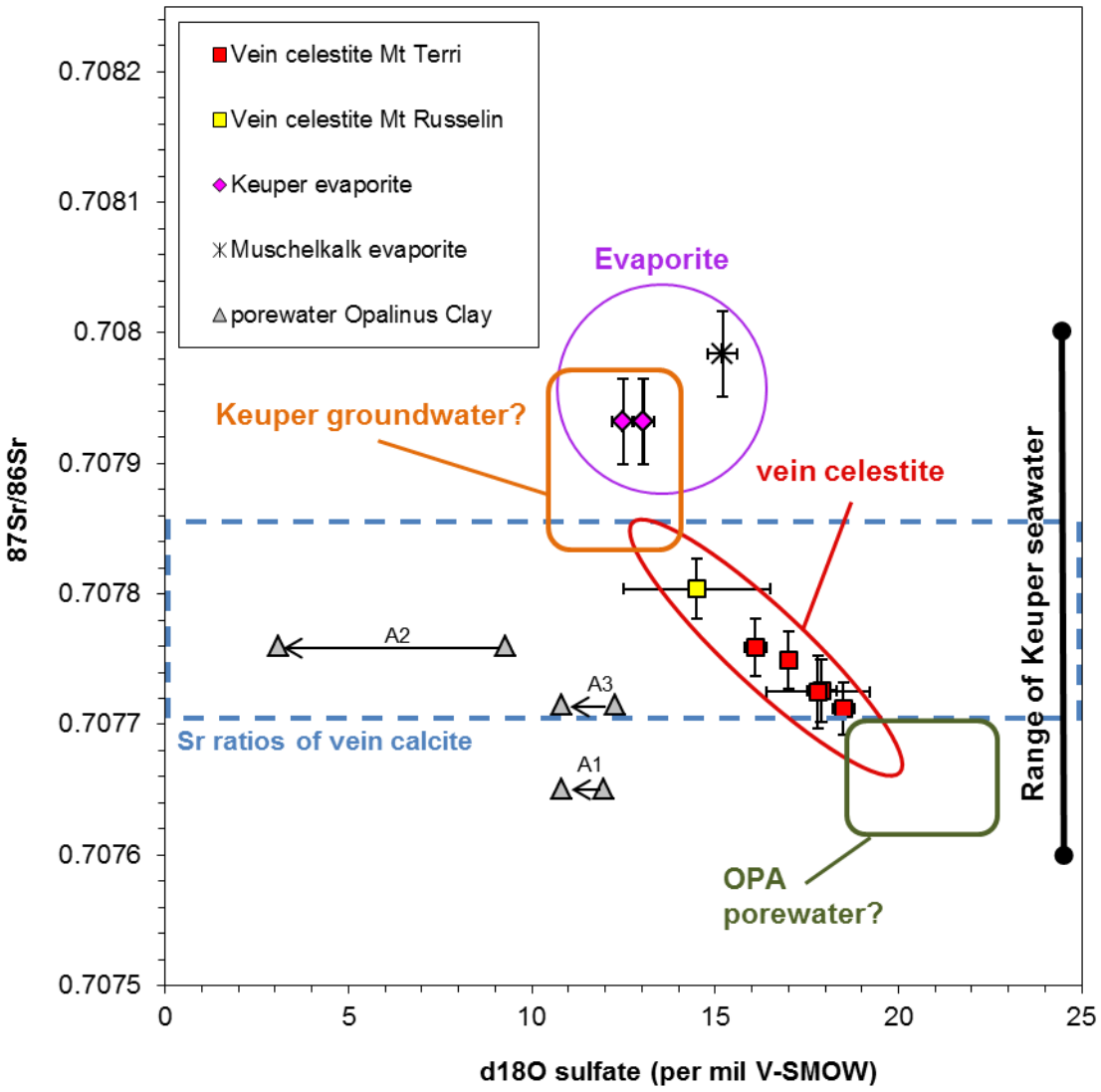

Fig. 4-6: The $^{87}Sr/^{86}Sr$ ratio versus $\delta^{18}O$ value of the sulfate of vein celestite in Opalinus Clay, of evaporitic gypsum and anhydrite in Keuper and Muschelkalk, and of Opalinus Clay porewater (boreholes BWS-A1 to A3; Pearson et al. 2003). Arrows between pairs of porewater data points indicate first and second sampling in each borehole. Variations are likely due to redox reactions during or before sampling and suggest $\delta^{18}O$ values are not reliable. Any contribution from pyrite oxidation would shift the $\delta^{18}O$ to more positive values. Data for porewater Sr isotopes are in most cases from different samples. The range of $^{87}Sr/^{86}Sr$ ratio for Keuper seawater is from McArthur et al. (2001). The dashed box shows the range of Sr isotope composition of vein calcite. The data for vein celestite correlate along a mixing line possibly connecting Keuper groundwater with Opalinus Clay (OPA) porewater (see text for discussion).

5. Discussion

5.1 Mineralogy and petrography

Veins with calcite and/or celestite were found from the base of the Opalinus Clay up to the Malm limestone. Calcite is ubiquitous in the studied veins but the presence of celestite is restricted to the Opalinus Clay. Sampling was denser in the vicinity of the Main Fault in the Opalinus Clay, and the used washing method was very successful to recover small vein fragments, bioclasts, and diagenetic sulfides. Samples within the Main Fault (Opalinus Clay) show abundant veinlets (≤ 1mm thick) of calcite locally associated with celestite and pyrite, the latter being possibly in part mechanically recycled diagenetic pyrite. Veins hosted by Opalinus Clay outside the Main Fault tend to be thicker (up to 2 cm), are generally oriented perpendicular to the fold axis or sub-horizontal, and always bear celestite.

Occurrences of fibrous calcite and celestite (Figs. 3-2 and 3-4A,B) in veins provide evidence for syntectonic (synkinematic) precipitation. Late tectonic activity with respect to vein mineralization is recorded by shear extensional jogs cutting veins, partially filled by late stage calcite and celestite (Fig. 3-3), and by the presence of stylolite joints in vein calcite in the Malm limestone that indicate a peak of compressive stress after vein formation. These data indicate that veins in the Opalinus Clay and Malm limestone formed during a major tectonic event, most likely the Jura folding and thrusting.

Most sulfides in the Opalinus Clay are of diagenetic origin, as the very fine-grained pyrite is a typical product of bacterial sulfate reduction. The presence of sphalerite was unexpected and suggests that clay minerals were sorbing significant amounts of Zn that might have been liberated to the porewater and fixed as sphalerite when the redox state of the porewater dropped in response to bacterial sulfate reduction. The fact that sphalerite is enclosed by diagenetic calcite both in sandy layers and shell-rich horizons suggest it is, like pyrite, an early diagenetic phase. Pyrite (and sphalerite) is commonly found in fossil shells, and this is consistent with an origin through bacterial reduction of seawater sulfate, a process that needs nutrients (the dead organisms). No clear evidence for post-diagenetic sulfide precipitation has been found in the investigated sections that could correspond to a later hydrothermal event (e.g. fluid flows through the veins). The content of sulfide minerals in the celestite-calcite vein of borehole BSF-004 is insignificant and might be in large part mechanically recycled from the wall rock.

Celestite solubility increases with decreasing temperature and increasing pressure and salinity (Rimstidt 1997). Thus, celestite precipitation can occur as a result of fluid heating, pressure drop or dilution through mixing with low salinity fluid. Because the solubility of celestite with temperature is concave upward, mixing of two celestite-saturated solutions at different temperatures would produce a supersaturated solution, which can lead to fast precipitation. However, the temperature difference between deep (Trias) and shallow (Malm) aquifers was probably between 10 and 15°C (considering a gradient of 30°C/km) and this relatively small gradient might not be relevant. Precipitation through pressure drop can occur when a deep overpressured aquifer suddenly leaks upward through a fault. Alternatively, mixing of a sulfate-rich with a Sr-rich fluids is a very effective way for celestite precipitation. It is important to note that vein celestite is only found in clay-rich rocks (Opalinus Clay). It is therefore likely that celestite precipitated through interaction between a sulfate-rich fluid (externally sourced) and the Sr sorbed on clay minerals.

Like celestite, calcite solubility decreases with increasing temperature. It is strongly controlled by the partial pressure of CO_2 and therefore total pressure and pH (Rimstidt 1997). At low temperatures (<100°C) and constant CO_2 pressure, solubility decreases when salinity increases. Below 100°C, calcite can be efficiently precipitated through the mixing of two fluids at different temperatures and/or salinities, or through pressure drop (CO_2 degassing).

Possible reservoirs of mineralizing fluids include the Trias (Keuper and Muschelkalk), the Opalinus Clay (porewater), and the the Dogger-Malm limestone aquifer. Possible sulfate sources include the Trias evaporite (gypsum and anhydrite, through dissolution) and seawater-derived fluids rich in SO_4 (porewater or groundwater).

Tertiary deposits are in most parts of the area eroded after Jura folding and thrusting and it is not trivial to assess if and where seawater was present during that time interval in the area. The youngest marine sediments documented in the St Ursanne area (Laubscher, 1963) are Oligocene (Stampian, or Rupelian), and consist of marine conglomeratic sand and molasses. Miocene sediments are absent from the St Ursanne area but occur in the nearby eastern Movelier-Soyhières-Delémont-Courrendlin sheet (Liniger & Keller, 1930), where rare Helvetian marine sediments are recorded. A more regional overview of the evolution of the sedimentation in the area during the Tertiary can be found in Kuhlemann & Kempf (2002).

In the sections below we discuss first the characterization of the fluid reservoirs based on the large whole rock isotopic profiles and data from disseminated minerals, and then the data obtained from vein minerals.

5.2 Isotope signatures in wallrocks

5.2.1 Sulfur isotopes

The wide distribution of $\delta^{34}S$ values for pyrite (and sphalerite) observed in Fig. 4-1 is typical for diagenetic sulfides produced by bacterial reduction of seawater sulfate during early diagenesis. However, most of the published data of bulk diagenetic pyrite in sediments show values at -25‰ ±20‰, with a mean of about -25‰ and a median at about -20‰ (Ohmoto and Goldhaber 1997). Data from Mont Terri are centered at about 0‰, which is therefore higher than average documented diagenetic pyrite in sediments. The $\delta^{34}S$ of seawater sulfate varied from about +17 ‰ during the Triassic down to +15 ‰ during the Jurassic (Claypool et al. 1980). These values are far below the maximum $\delta^{34}S$ value (+57.8 ‰) obtained on pyrite from sediments of Mont Terri and Mont Russelin of the corresponding ages. Rayleigh distillation is required to obtain sulfide $\delta^{34}S$ values that are above the initial sulfate source. This implies that bacterial seawater sulfate reduction took place under nearly closed conditions for SO_4^{--} (but open for H_2S through pyrite precipitation and/or diffusion), with the diffusion rate of seawater sulfate into the sediments being slower than the reduction rate. This is a common feature in clay-rich sediments with low permeability and the main result is that virtually no Jurassic formation seawater sulfate is likely to have been preserved in the porewater of the Opalinus Clay after early diagenesis (sulfate content of porewater in reduced sediments is commonly of the order of 0.001 molal, i.e. 100 mg/l; e.g. Ohmoto and Goldhaber 1997; Böttcher et al. 2006). However, Pearson et al. (2003) reported present day sulfate concentrations in Opalinus Clay porewater at Mont Terri of up to about 2000 mg/l, with correlation of the sulfate and chloride contents at a ratio similar to present day seawater (present day seawater contains 2710 mg/l dissolved SO_4; Clark & Fritz 1997). This suggests that the sulfate presently found in the Opalinus Clay porewater diffused in from an external

source, after early diagenesis and pyrite precipitation. Fig. 4-2 suggests that present day isotopic composition of the porewater sulfate is similar to Miocene seawater. However, the only known evidence of Tertiary seawater sedimentation in the St Ursanne area is during the Oligocene, and rare Miocene sediments are only known further to the East (Laubscher 1963; Liniger & Keller, 1930). Downward diffusion and equilibration of sulfate and chloride derived from Tertiary seawater in the Opalinus Clay is furthermore problematic because the time needed to reach equilibrium would probably be huge, except if the Malm aquifer could have been connected directly to the sea through tectonic or erosional structures. It has already been discussed that the isotopic data for the Opalinus Clay porewater are apparently perturbed by redox reactions and might be significantly shifted towards more negative values due to pyrite oxidation (source of sulfate). The present day isotopic composition of the Opalinus Clay porewater sulfate is therefore poorly constrained, and its source, although clearly not the Jurassic formation seawater, cannot be sorted out from whole rock data.

5.2.2 Strontium isotopes

The $^{87}Sr/^{86}Sr$ ratio of whole rock carbonate obtained from limestone, dolostone, or evaporite sulfate broadly fits with values published for the seawater Sr at the time of sedimentation. In contrast, clay-rich rocks show a more radiogenic $^{87}Sr/^{86}Sr$ ratio. The origin of this shift is not solved and probably reflects a mixed signal involving Sr in carbonate minerals, Sr sorbed on clay minerals, pore-water Sr, and possibly Sr released by silicate minerals dissolution. At this stage, further methodology work is needed to better constrain the different Sr contributors during the acetic acid leach of the rock, and possibly improve the procedure.

The profile of whole-rock carbonate $^{87}Sr/^{86}Sr$ values in the Opalinus Clay might suggest some kind of lowering in and near the Main Fault, down to values similar to vein minerals (Fig. 4-5). This could indicate some perturbation related to the past fluid flow in the Main Fault, but because of the uncertainty regarding the exact meaning of the $^{87}Sr/^{86}Sr$ ratio obtained by the acetic acid leach of clay-rich rocks, any interpretation is considered to be irrelevant at this stage of understanding and level of sampling density.

5.2.3 Oxygen and carbon isotopes of carbonate

Without considering the Main Fault area, which might be perturbed by past fluid flows, the $\delta^{18}O$ values of whole rock carbonate range between about 24 and 29 ‰ V-SMOW from the Trias to the Malm. This is at or slightly below the expected equilibrium of calcite with seawater at tropical temperatures (O'Neil et al. 1969) and suggests some degree of diagenetic overprint. The $\delta^{13}C$ values of whole rock carbonate are essentially positive across the whole profile, between about 0 and 3‰ V-PDB, except for one sample (BWS-E9) plotting at about -3‰ V-PDB. This sample is located at the top of the Keuper and is rich in marcasite and black shale, and biogenic carbon is clearly present.

5.3 Isotope signatures in veins

5.3.1 Oxygen and carbon isotopes of vein calcite

The $\delta^{18}O$ of vein calcite is systematically lower than that of whole-rock carbonate (Fig. 4-5A), and this indicates precipitation at higher temperatures than during sedimentation and/or a meteoric component in the mineralizing fluids (not pure seawater). Obtained values would fit

with temperatures up to 100°C (using equation of O'Neil et al. 1969) if seawater was involved or, more likely, lower temperature if meteoric water was mixed with seawater. The $\delta^{13}C$ of vein calcite is variable, and aside from a vein sample located at the base of the Opalinus Clay, all vein calcite are more negative than their host rock carbonate (Fig. 4-5B). Interestingly, the $\delta^{13}C$ of the whole rock carbonate of the Opalinus Clay near and within the Main Fault is low, and this suggests some overprint by fluids bearing carbon with negative $\delta^{13}C$ values. Similarly, the $\delta^{18}O$ of the whole rock carbonate near and within the Main Fault apparently shows some lowering, but not so clearly as for $\delta^{13}C$ (Fig. 4-5A).

5.3.2 Sulfur and oxygen isotopes of sulfide and sulfate minerals in veins

Diagenetic pyrite tends to show lower $\delta^{34}S$ values in the Main Fault zone (Fig. 4-3), but it is not clear if this tendency is due to an overprint by post-diagenetic sulfate-rich (part of it can be reduced in situ and produce isotopically light pyrite) fluids circulating in the fault or if it is a bias from sampling, because the Main Fault has been sampled in much more detail for diagenetic pyrite.

The sulfur and oxygen isotope data (Fig. 4-2) of sulfate in vein celestite are broadly arranged on a trend that would be compatible with variable degrees of bacterial reduction (Fritz et al. 1989, Canfield 2001, Turchyn et al. 2006) of Jurassic, Keuper, or Muschelkalk sulfate, or with mixing between two sulfate sources; one dominated by Jurassic or Triassic sulfate and the other by seawater sulfate modified by bacterial reduction (of unclear age).

5.3.3 Strontium isotopes of vein calcite and celestite

The $^{87}Sr/^{86}Sr$ ratios of vein calcite and celestite are comparable, and nearly constant (0.7077 to 0.70785) from the bottom of the Opalinus Clay up to the Malm limestone (Fig. 4-5C), which suggests fluids flowed across the Mesozoic sequence and were apparently dominated by one Sr source.

The $^{87}Sr/^{86}Sr$ ratios of vein minerals (0.70770 to 0.70785) partly overlap values of present day porewater in the Opalinus Clay (Pearson et al. 2003), fit within the range of worldwide Keuper sediments (0.7076 to 0.708; McArthur et al. 2001), and are close to the values obtained for Trias evaporite (gypsum and anhydrite) at Mont Terri (Fig. 4-6).

Vein values are significantly lower than the $^{87}Sr/^{86}Sr$ ratio of the Burdigalian seawater during the deposition of the Upper Marine Molasse (OMM) if considering the global oceanic value (0.7078 to 0.7088; McArthur et al. 2001), and therefore exclude any contribution from such source, as has been documented in veins found in the Oftringen borehole (de Haller et al. 2011; Mazurek et al. 2012). Another possibility could be a contribution from descending Rupelian (Oligocene) seawater (0.70783 to 0.7082; McArthur et al. 2001), but overlap is very limited and such contribution would be hard to reconcile with structural and textural evidences indicating vein formation occurred during the Jura folding and thrusting, which is at least about 20 Ma younger. On the other hand, a local source dominated by Jurassic seawater or carbonates would give much lower $^{87}Sr/^{86}Sr$ ratios (Fig. 4-5C) and is therefore not viable.

In a first approximation, obtained results suggest that the Sr of vein minerals is dominantly derived from Triassic sediments. Going into more details, Fig. 4-6 shows a correlation between the $\delta^{18}O$ of sulfate and the $^{87}Sr/^{86}Sr$ ratio of celestite, which indicates mixing between two well mixed reservoirs. One of the end-members might well correspond to Keuper groundwater, as the mixing trend apparently intersects the values obtained for Keuper gypsum. The other end-member likely corresponds to the Opalinus Clay porewater, because celestite is only found in the Opalinus Clay and this implies a local source.

As discussed before, Opalinus Clay porewater Sr isotope data and dissolved sulfate $\delta^{18}O$ values obtained by Pearson et al. (2003) are questionable because redox reactions clearly occurred before or during sampling. When considering the data obtained from vein celestite, it is interesting to note that there is no correlation between the $^{87}Sr/^{86}Sr$ ratios and the $\delta^{34}S$ values of celestite, which means $\delta^{34}S$ is in part decoupled from $\delta^{18}O$. This is visible in Fig. 4-2, where the isotopic data of vein sulfate (celestite and barite) are much less correlated at higher $\delta^{18}O$ and $\delta^{34}S$ values. Such decoupling has been documented in present day porewaters (Böttcher et al. 1999; Turchyn et al. 2006) where the $\delta^{18}O$ of dissolved sulfate increases rapidly and then stabilizes at values between +22 and +25 ‰ (V-SMOW) while $\delta^{34}S$ continues to increase as a response to bacterial sulfate reduction. These observations suggest that the Opalinus Clay porewater at the time of celestite precipitation was bearing sulfate with variable $\delta^{34}S$ but apparently fixed $\delta^{18}O$ and $^{87}Sr/^{86}Sr$ ratio, this one being slightly lower than Keuper evaporite (Fig. 4-6) but above Aalenian seawater, possibly reflecting a mixing between these two sources.

To conclude, celestite precipitation may have resulted from the mixing between fluids sourced within the Keuper aquifer and Opalinus Clay porewater. If this interpretation is correct, a significant proportion of the Sr contained in the Opalinus Clay porewater (and sorbed on clay minerals) and all or most of its dissolved sulfate also originated from the Keuper through slow diffusion. The isotope composition of the sulfate diffused into the Opalinus Clay has been modified by bacterial sulfate reduction within the Opalinus Clay or in the Lias units, probably at a sufficiently slow rate to allow reaching a fixed $\delta^{18}O$ value (Fritz et al. 1989; Böttcher et al. 1999; Turchyn et al. 2006). This diffusion process might have taken place already at the time of Opalinus Clay deposition and might still be active today. Similar upward diffusion of sulfate in porewater from underlying sedimentary units has already been described by Böttcher et al. (1999 and 2006).

No isotopic evidences were found that indicate the involvement of a chemically distinct (and therefore recognizable) input from a possible Dogger-Malm groundwater during the vein formation.

5.4 Solute transport and precipitation mechanisms of vein minerals

The obtained data suggest that fluids sourced within the Trias, probably the Keuper, crossed the Opalinus Clay through faults that were active during the Jura folding. Such fluid flow is typically pulsed and related to seismic movements (e.g. Cox 2005). It is transient because the pressures of the involved aquifers tend to equilibrate when connected and because the fractures tend to self-seal. The main sealing mechanisms include vein mineral precipitation, swelling of clays, and ductile behavior of clay-rich rocks.

Likely precipitation mechanisms of vein minerals at Mont Terri include pressure drop and fluid mixing, including interaction with Opalinus Clay porewater.

The results of this study show that fluid flow and vein formation was apparently restricted to a time of intense tectonic activity (the Jura folding and thrusting). Aside from this particular geotectonic context, the Opalinus Clay apparently behaved as a stable seal and solute transport was (and is nowadays; see Pearson et al. 2003) dominated by diffusion.

6. Conclusions

Data for Sr, O, C, and S isotopes, when combined with petrographic and tectonic evidences, suggest that veins found at Mont Terri belong to a single mineralizing event, most likely related to the Jura folding and thrusting. The presence of veins is restricted to the NE trending Main Fault thrust and to NW and NE structures that were active during the Jura folding and thrusting.

Sulfate-rich fluids were apparently expelled upward from the Trias aquifers (probably Keuper) through active faults and mixed with local fluids. The deep Triassic source is relatively well constrained by the strontium, sulfur, and oxygen isotopes of vein celestite, and the same data suggest the Opalinus Clay porewater was a key contributor for the precipitation of vein celestite. No data are available for the Sr and dissolved sulfate isotopic composition of the groundwater that might have been present in the Dogger-Malm at the time of vein formation and no particular isotopic imprint on the vein minerals from this aquifer has been observed. The involvement of downward flowing Tertiary seawater is not supported by the data and the geological background.

Some degree of perturbation of the rock properties is observed in the Opalinus Clay in and near the Main Fault. This perturbation apparently reflects the imprint of the fluids that produced the vein mineralizations and consists of a lowering of the $\delta^{13}C$ value of the whole rock carbonate towards the values of vein calcite. In addition, weak or not straightforward lowering of the $\delta^{18}O$ value and $^{87}Sr/^{86}Sr$ ratio of the whole rock carbonate, and a depletion of the $\delta^{34}S$ of the diagenetic pyrite are observed, but doubt remains on their significance. It follows that whole rock $\delta^{13}C$ (and possibly $\delta^{18}O$) profiles across major tectonic structures might be used to highlight past fluid flow in clay-rich rocks. The use of the $^{87}Sr/^{86}Sr$ ratio of whole rock carbonate might also be effective but it is probably not reliable (or at least understood) in clay-rich rocks due to the discussed methodological problems associated with the acetic acid leach technique.

This study suggests that the Opalinus Clay acted as a stable seal during most of its existence, except during the Jura folding and thrusting, sometime within the period 10–3 Ma ago, when tectonic strain induced transient fluid flows and mineralization in faults cutting across the Mesozoic units. Aside from this period of intense tectonic activity, solute transport in the Opalinus Clay has probably been dominated by diffusion, as this is the case at present. In today's situation, no hydrogeological or porewater geochemical perturbations are recorded in the Main Fault area, and this gives further support in favor of an efficient self-sealing capacity.

Sulfur isotope results obtained during this study on diagenetic pyrite from the Opalinus Clay show highly positive $\delta^{34}S$ values up to +58 per mil V-CDT that indicate almost complete bacterial seawater sulfate reduction in the porewater during early diagenesis. However, other studies showed that present day porewater has a sulfate/chloride ratio similar to today's seawater and concentrations that approach seawater. It is clear from sulfur isotopes of diagenetic pyrite that the present-day sulfate content of the Opalinus Clay porewater is not inherited from the formation seawater at the time of sedimentation, and isotope data on vein celestite suggest sulfate and strontium might have diffused in the porewater from the underlying Trias evaporite, probably since sedimentation time.

7. References

Balci, N., Shanks III, W.C., Mayer B., Mandernack, K.W., 2007, Oxygen and sulfur isotope systematics of sulfate produced by bacterial and abiotic oxidation of pyrite. Geochimica and Cosmochimica Acta, v. 71, p. 3796-3811

Balderer, W., Pearson, F.J.J., and Soreau, S., 1991, Sulphur and oxygen isotopes in sulphate and sulphide: in Pearson, F.J.Jr., Balderer, W., Loosli, H.H., Lehmann, B.E., Matter, A., Peters, Tj., Schmassmann, H., Gautschi, A., eds., Applied isotope hydrology: A case study in northern Switzerland: Studies in Environmental Science, Elsevier, Amsterdam, v. 43, p. 297-325

Bock, H., Dehandschutter, B., Martin, C.D., Mazurek, M., de Haller, A., Skoczylas, F. and Davy, C., 2010, Self-sealing of fractures in argillaceous formations in context with the geological disposal of radioactive waste. OECD/NEA report 6184, OECD Nuclear Energy Agency, Paris, France. 310 p.

Bossart, P., and Thury, M., 2008, Mont Terri Rock Laboratory. Project, programme 1996 to 2007 and results. Wabern: Reports of the Swiss Geological Survey no. 3

Böttcher, M.E., Bernasconi, S.M., and Brumsack, H.-J., 1999, Carbon, sulfur, and oxygen isotope geochemistry of interstitial waters from the western Mediterranean. In Zahn, R., Comas, M.C., and Klaus, A. (Eds.), Proceedings of the Ocean Drilling Program, Scientific Results, vol. 161, p. 413-421

Böttcher, M,E., Ferdelman, T.G., Jørgensen, B.B., Blake, R.E., Surkov, A.V., and Claypool, G.E., 2006, Sulfur isotope fractionation by the deep biosphere within sediments of the eastern equatorial Pacific and Peru margin. *In* Jørgensen, B.B, D'Hondt, S.L., Miller, D.J. (Eds.), Proceedings of the Ocean Drilling Program (ODP), Scientific Results, v. 201, p. 1-21 (online)

Canfield, D.E., 2001, Biogeochemistry of sulfur isotopes. In: J.W. Valley and D. Cole, eds., Reviews in Mineralogy and Geochemistry, v. 43, p. 607-636

Clark, I. and Fritz, P., 1997, Environmental Isotopes in Hydrogeology. Lewis Publishers, Boca Raton and New York, 328 pp.

Clauer, N., 2011, SF (Self-sealing of faults and paleo-fluid flow) experiment: Report on the study made in the frame of the self-sealing project. Mont Terri Technical Note TN 2010-43

Claypool, G.E., Holser, W.T., Kaplan, I.R., Sakai, H., and Zak, I., 1980, The age curves of sulfur and oxygen isotopes in marine sulfate and their mutual interpretation: Chemical Geology, v. 28, p. 199-260

Cox, S.F., 2005, Coupling between deformation, fluid pressure, and fluid flow in ore-producing hydrothermal systems at depth in the crust. Economic Geology 100th Anniversary Volume, p. 39-75

de Haller, A., Tarantola, A., MAzurek, M., and Spangenberg, J., 2011, Fluid flow through the sedimentary cover in northern Switzerland recorded by calcite-celestite veins (Oftringen borehole, Olten). Swiss Journal of Geoscience, v. 104, p. 493-506

Diebold, P., Laubscher, H.P., Schneider, A., & Tschopp, R., 1963, Geologischer Atlas der Schweiz 1:25'000: Atlasblatt 40, 1085 St Ursanne. Schweizerische Geologische Kommission

Farmer, G.L., and Depaolo, D.J., 1997, Sources of hydrothermal components: Heavy isotopes: in Barnes, H.L., ed., Geochemistry of hydrothermal ore deposits, third edition: J. Wiley & sons, p. 31-61

Faure, G., 1986, Principles of isotope geology, 2nd edition. Whiley, New York, 589 p.

Fisher, Q., Kets, F., and Crook, A., 2011, Self-sealing of faults and fractures: Evidence from the petroleum industry. Nagra Arb. Ber. NAB 13-06

Fritz, P., Basharmal, G.M., Drimmie, R.J., Ibsen, J., and Qureshi, R.M., 1989, Oxygen isotope exchange between sulphate and water during bacterial reduction of sulphate: Chemical Geology (Isotope Geoscience Section), v. 79, p. 99-105

Giesemann, A., Jager, H.J., Norman, A.L., Krouse, H.P., and Brand, W.A., 1994, Online sulfur isotope determination using an elemental analyzer coupled to a mass-spectrometer. Analytical Chemistry, v. 66, p. 2816-2819

Kuhlemann, J., & Kempf, O., 2002, Post-Eocene evolution of the North Alpine Foreland Basin and its response to alpine tectonics. Sedimentary Geology, v. 152, p. 45-78

Laubscher, H.P., 1963, Atlas Géologique de la Suisse 1:25 000: Atlasblatt 40, 1085 St Ursanne ; Erläuterungen. Schweizerische Geologische Kommission, Organ der Schweiz. Naturforsch. Gesellschaft

Lerouge, C., Gaboreau, S., Blanc, P., Guerrot, C., Haas, H., Jean-Prost, V., Touzelet, S., and Wille, G., 2010, PC-C Experiment : Mineralogy and geochemistry of cores of the BP-C2 borehole. Mont Terri Consortium Technical Note TN 2010-05, St Ursanne, Switzerland

Liniger, H., & Keller, W.T., 1930, Atlas Géologique de la Suisse 1:25 000: Atlasblatt 1, 92 Movelier, 93 Soyhières, 94 Delémont, 95 Courrendlin ; Erläuterungen. Geologische Kommission der Schweiz. Naturforsch. Gesellschaft

McArthur, J.M., Howarth, R.J., & Bailey, T.R., 2001, Strontium isotope stratigraphy: LOWESS Version 3: Best fit to the marine Sr-isotope curve 0-509 Ma and accompanying look-up table for deriving numerical age. Journal of Geology, v. 109, p. 155-170

Mazurek, M., Koroleva, M., and Müller, H., 2009, Boreholes BWS-H1 and BWS-H2: Results of the mineralogical and petrological laboratory programme. Mont Terri Project Technical note 2009-14

Mazurek, M., Möri, A., and Nussbaum, C., 2010, Self sealing (SF) project: Geological framework, drilling and evaluation of pilot and sampling drillcores. Mont Terri Project Technical note 2006-71

Mazurek, M., Waber, H.N., Mäder, Gimmi, T., De Haller, A. & Koroleva, M. (2012). Geochemical Synthesis for the Effingen Member in Boreholes at Oftringen, Gösgen and Küttigen. Nagra Technical Report NTB 12-07

Meier, P.M.; Trick, Th.; Blümling, P. and Volckaert, G., 2002, Self-healing of fractures within the EDZ at the Mont Terri Rock Laboratory: results after one year of experimental work. – In: Hoteit, N.; Su, K.; Tijani, M. and Shao, J.-F. (Eds.): Hydromechanical and thermohydromechanical behaviour of deep argillaceous rocks. – Intern. Workshop, Paris, 11-12 Oct. 2000, p. 267-274, Lisse (Swets & Zeitlinger)

Nussbaum, C., Bossart, P., Amann, F., and Aubourg, C., 2011, Analysis of tectonic structures and excavation induced fractures in the Opalinus Clay, Mont Terri underground laboratory (Switzerland). Swiss Journal of Geosciences, v. 104, p. 187-210

Ohmoto, H., and Goldhaber, M.B., 1997, Sulfur and carbon isotopes: in Barnes, H.L., ed., Geochemistry of hydrothermal ore deposits, third edition: J. Wiley & sons, p. 517-611

O'Neil, J.R., Clayton, R.N., & Mayeda, T.K., 1969, Oxygen isotope fractionation in divalent metal carbonates. Journal of Chemistry and Physics, v. 51, p. 5547-5558

Pearson F.J., Arcos D., Bath A., Boisson J.Y., Fernandez A.M., Gaebler H.E., Gaucher E.C., Gautschi A., Griffault L., Hernan P. and Waber H.N., 2003, Mont Terri Project – Geochemistry of Water in the Opalinus Clay Formation at the Mont Terri Rock Laboratory. Reports of the Federal Office of Water and Geology (FOWG), Geology Series No. 5

Pilot, J., Rosler, H.J., and Muller, P., 1972, Zur geochemischen Entwicklung des Meerwassers und mariner Sedimente im Phanerozoikum mittels Untersuchungen von S-, O- und C-Isotopen: Neue Bergbautechnik, v. 2, p. 161-168

Rimstidt, J.D., 1997, Gangue mineral transport and deposition. In H.L. Barnes, (Ed.), Geochemistry of hydrothermal ore deposits, 3rd edition, J. Wiley & Sons, p. 487-515

Seal, II, R.R., Alpers, C.N., and Rye, R.O., 2000, Stable isotope systematics of sulfate minerals: in Alpers, C.N., Jambor, J.L., and Nordstrom, D.K., eds., Sulfate Minerals: crystallography, geochemistry, and environmental significance, Reviews in Mineralogy & Geochemistry, v. 40, p. 541-602

Stroes-Gascoyne, S., Sergeant, C., Schippers, A., Hamon, C.J., Nèble, S., Vesvres, M.-H., Barsotti, V., Poulain, S., and Le Marrec, C., 2011, Biogeochemical processes in a clay formation in situ experiment: Part D – Microbial analyses – Synthesis of results. Applied Geochemistry, vol. 26, p. 980-989

Taylor, H.P.Jr., 1997, Oxygen and hydrogen isotope relationships in hydrothermal mineral deposits: in Barnes, H.L., ed., Geochemistry of hydrothermal ore deposits, third edition: J. Wiley & sons, p. 229-302

Turchyn, A.V., Sivan, O., and Schrag, D.P., 2006, Oxygen isotopic composition of sulfate in deep sea pore fluid: evidence for rapid sulfur cycling: Geobiology, v. 4, p. 191-201

Waber, H.N., ed., 2008, Borehole Oftringen: Mineralogy, porosimetry, geochemistry, porewater chemistry. Nagra NAB 08-18, 276 p.

Waber, H.N. & Schürch, R., 2000, WS-A Experiment: Fracture mineralogy and geochemistry as constraints on porewater composition. Mont Terri Consortium Report, St Ursanne, Switzerland

Wersin, P., Mazurek, M., Waber, H.N., Mäder, U.K., Gimmi, Th., Rufer, D., de Haller, A., and Bläsi, H.R., 2013, Rock and porewater characterization on drillcores from the Schlattingen-1 borehole. Nagra Arbeitsbericht NAB 12-54